MOLECULAR IMAGING WITH THE SCANNING TUNNELING MICROSCOPE

BY

YOU HUAN YEO

A THESIS SUBMITTED TO THE FACULTY OF GRADUATE STUDIES IN PARTIAL FULFILLMENT OF THE REQUIREMENTS FOR THE DEGREE OF

DOCTOR OF PHILOSOPHY

DEPARTMENT OF ELECTRICAL AND COMPUTER ENGINEERING

UNIVERSITY OF MANITOBA, WINNIPEG, MANITOBA

ISBN 0-315-99014-7

Name You Huan YEO

Dissertation Abstracts International is arranged by broad, general subject categories. Please select the one subject which most nearly describes the content of your dissertation. Enter the corresponding four-digit code in the spaces provided.

Electronics & Electrical
SUBJECT TERM

0544
SUBJECT CODE

U·M·I

Subject Categories

THE HUMANITIES AND SOCIAL SCIENCES

COMMUNICATIONS AND THE ARTS
Architecture 0729
Art History 0377
Cinema 0900
Dance 0378
Fine Arts 0357
Information Science 0723
Journalism 0391
Library Science 0399
Mass Communications 0708
Music 0413
Speech Communication 0459
Theater 0465

EDUCATION
General 0515
Administration 0514
Adult and Continuing 0516
Agricultural 0517
Art 0273
Bilingual and Multicultural 0282
Business 0688
Community College 0275
Curriculum and Instruction 0727
Early Childhood 0518
Elementary 0524
Finance 0277
Guidance and Counseling 0519
Health 0680
Higher 0745
History of 0520
Home Economics 0278
Industrial 0521
Language and Literature 0279
Mathematics 0280
Music 0522
Philosophy of 0998
Physical 0523
Psychology 0525
Reading 0535
Religious 0527
Sciences 0714
Secondary 0533
Social Sciences 0534
Sociology of 0340
Special 0529
Teacher Training 0530
Technology 0710
Tests and Measurements 0288
Vocational 0747

LANGUAGE, LITERATURE AND LINGUISTICS
Language
- General 0679
- Ancient 0289
- Linguistics 0290
- Modern 0291

Literature
- General 0401
- Classical 0294
- Comparative 0295
- Medieval 0297
- Modern 0298
- African 0316
- American 0591
- Asian 0305
- Canadian (English) 0352
- Canadian (French) 0355
- English 0593
- Germanic 0311
- Latin American 0312
- Middle Eastern 0315
- Romance 0313
- Slavic and East European 0314

PHILOSOPHY, RELIGION AND THEOLOGY
Philosophy 0422
Religion
- General 0318
- Biblical Studies 0321
- Clergy 0319
- History of 0320
- Philosophy of 0322

Theology 0469

SOCIAL SCIENCES
American Studies 0323
Anthropology
- Archaeology 0324
- Cultural 0326
- Physical 0327

Business Administration
- General 0310
- Accounting 0272
- Banking 0770
- Management 0454
- Marketing 0338

Canadian Studies 0385
Economics
- General 0501
- Agricultural 0503
- Commerce-Business 0505
- Finance 0508
- History 0509
- Labor 0510
- Theory 0511

Folklore 0358
Geography 0366
Gerontology 0351
History
- General 0578
- Ancient 0579
- Medieval 0581
- Modern 0582
- Black 0328
- African 0331
- Asia, Australia and Oceania 0332
- Canadian 0334
- European 0335
- Latin American 0336
- Middle Eastern 0333
- United States 0337

History of Science 0585
Law 0398
Political Science
- General 0615
- International Law and Relations 0616
- Public Administration 0617

Recreation 0814
Social Work 0452
Sociology
- General 0626
- Criminology and Penology ... 0627
- Demography 0938
- Ethnic and Racial Studies 0631
- Individual and Family Studies 0628
- Industrial and Labor Relations 0629
- Public and Social Welfare 0630
- Social Structure and Development 0700
- Theory and Methods 0344

Transportation 0709
Urban and Regional Planning 0999
Women's Studies 0453

THE SCIENCES AND ENGINEERING

BIOLOGICAL SCIENCES
Agriculture
- General 0473
- Agronomy 0285
- Animal Culture and Nutrition 0475
- Animal Pathology 0476
- Food Science and Technology 0359
- Forestry and Wildlife 0478
- Plant Culture 0479
- Plant Pathology 0480
- Plant Physiology 0817
- Range Management 0777
- Wood Technology 0746

Biology
- General 0306
- Anatomy 0287
- Biostatistics 0308
- Botany 0309
- Cell 0379
- Ecology 0329
- Entomology 0353
- Genetics 0369
- Limnology 0793
- Microbiology 0410
- Molecular 0307
- Neuroscience 0317
- Oceanography 0416
- Physiology 0433
- Radiation 0821
- Veterinary Science 0778
- Zoology 0472

Biophysics
- General 0786
- Medical 0760

EARTH SCIENCES
Biogeochemistry 0425
Geochemistry 0996
Geodesy 0370
Geology 0372
Geophysics 0373
Hydrology 0388
Mineralogy 0411
Paleobotany 0345
Paleoecology 0426
Paleontology 0418
Paleozoology 0985
Palynology 0427
Physical Geography 0368
Physical Oceanography 0415

HEALTH AND ENVIRONMENTAL SCIENCES
Environmental Sciences 0768
Health Sciences
- General 0566
- Audiology 0300
- Chemotherapy 0992
- Dentistry 0567
- Education 0350
- Hospital Management 0769
- Human Development 0758
- Immunology 0982
- Medicine and Surgery 0564
- Mental Health 0347
- Nursing 0569
- Nutrition 0570
- Obstetrics and Gynecology .. 0380
- Occupational Health and Therapy 0354
- Ophthalmology 0381
- Pathology 0571
- Pharmacology 0419
- Pharmacy 0572
- Physical Therapy 0382
- Public Health 0573
- Radiology 0574
- Recreation 0575
- Speech Pathology 0460
- Toxicology 0383

Home Economics 0386

PHYSICAL SCIENCES
Pure Sciences
Chemistry
- General 0485
- Agricultural 0749
- Analytical 0486
- Biochemistry 0487
- Inorganic 0488
- Nuclear 0738
- Organic 0490
- Pharmaceutical 0491
- Physical 0494
- Polymer 0495
- Radiation 0754

Mathematics 0405
Physics
- General 0605
- Acoustics 0986
- Astronomy and Astrophysics 0606
- Atmospheric Science 0608
- Atomic 0748
- Electronics and Electricity 0607
- Elementary Particles and High Energy 0798
- Fluid and Plasma 0759
- Molecular 0609
- Nuclear 0610
- Optics 0752
- Radiation 0756
- Solid State 0611

Statistics 0463

Applied Sciences
Applied Mechanics 0346
Computer Science 0984
Engineering
- General 0537
- Aerospace 0538
- Agricultural 0539
- Automotive 0540
- Biomedical 0541
- Chemical 0542
- Civil 0543
- Electronics and Electrical 0544
- Heat and Thermodynamics ... 0348
- Hydraulic 0545
- Industrial 0546
- Marine 0547
- Materials Science 0794
- Mechanical 0548
- Metallurgy 0743
- Mining 0551
- Nuclear 0552
- Packaging 0549
- Petroleum 0765
- Sanitary and Municipal 0554
- System Science 0790

Geotechnology 0428
Operations Research 0796
Plastics Technology 0795
Textile Technology 0994

PSYCHOLOGY
General 0621
Behavioral 0384
Clinical 0622
Developmental 0620
Experimental 0623
Industrial 0624
Personality 0625
Physiological 0989
Psychobiology 0349
Psychometrics 0632
Social 0451

MOLECULAR IMAGING WITH THE SCANNING TUNNELING MICROSCOPE

BY

YOU HUAN YEO

A Thesis submitted to the Faculty of Graduate Studies of the University of Manitoba in partial fulfillment of the requirements of the degree of

DOCTOR OF PHILOSOPHY

Abstract

The scanning tunneling microscope is used to study the structures of physisorbed organic molecules on solid surfaces. For *n*-decanol and *n*-dodecanol physisorbed at the liquid/graphite interface, the STM images show that the molecules lie parallel to the substrate surface and formed two-dimensional ordered array. Using the voltage dependent imaging mechanism, we are able to identify the locations of the hydroxyl groups of the molecules. Images of *n*-decanol molecules and graphite lattice are simultaneously obtained using the dual-bias technique, which shows that the substrate lattice can be imaged without disturbing the adsorbed layer. Imaging *n*-dodecanol molecules above the bulk melting temperature shows for the first time the two-dimensional structural phase transition of the adsorbed layer. We also examined the structures of *n*-decanol, *n*-dodecanol and octanoic acids molecules self-assembled at the liquid/Au(111) interface. The adsorbed layer exhibits a superlattice structure with respect to the underlying hexagonal array of 5 Å lattice parameter. A possible reconstruction of the Au(111) surface is observed when imaging *n*-dodecanols at various tunneling parameters. Some preliminary studies of the long chain *n*-$C_{26}H_{54}$ adsorbed on graphite in ultra high vacuum show that the molecules formed ordered array at room temperature. Finally, the imaging mechanism associated with STM imaging of molecules is discussed using a resonant tunneling model. The results indicate that in the case of imaging *n*-decanol molecules on graphite, although the molecular orbitals lie well above the Fermi level of graphite, a significant effect to the tunneling current from these molecular orbitals can be observed near the Fermi level.

Acknowledgments

I would like to thank my advisor Dr. Douglas J. Thomson for his excellent guidance and supervision throughout the last four years. He makes graduate study a fun thing to do. I am very grateful that he had faith in an underdog student when others did not.

It is a pleasure to thank Dr. Gordon McGonigal, my colleagues Kerry Yackoboski, Peter Guo and Ken Westra who have contributed a great deal of advice and practical help without which this work would not have arrived at this stage. Special thanks must be made to Dr. Jane E. Frommer, for the constant discussions and encouragement via e-mails.

Thanks are also due to the Mechanical and Electronic workshop personnel of the Department of Electrical and Computer Engineering for their advice and help during various stages of the research work.

"Two days ago I looked down through my sparkling microscope. Opened up the diaphragm for more light and there it was. I said my my, what's this, it moves.....I didn't think I'd tell the others but I had to. Great believer in the professional courtesy. Crowding round they said it was some crystalline salt. How could they be so cruel. I told them go away. I gave it the test for proteins. It passed."

----------J. P. Donleavy

Meet My Maker the Mad Molecule

Table of Contents

Figure Captions

Chapter 1
The Scanning Tunneling Microscope

1.1 Introduction

Frankfurt 1978, the idea of the scanning tunneling microscope (STM) for surface science research was born. This idea quickly became a reality at 2:00 a.m. on the 18 March 1981. The result is "Scanning tunneling microscopy, a novel technique based on vacuum tunneling, yields surface topographies in real space and work function profiles on a atomic scale" [1, 2]. The chief architects of the STM, Gerd Binnig and Heinrich Rohrer of IBM Zurich were soon awarded the Nobel prize for physics in 1986. The success of the STM in achieving atomically resolved images of surfaces has triggered the development of a variety of other scanning probe microscopes.

Still in its infancy, the STM has already established itself in the hierarchy of surface analytical techniques such as low energy electron diffraction and Auger electron spectroscopy, which provide a wealth of information about the surface but are inherently limited to the ultrahigh vacuum (UHV) environment. Although the first STM experiments were performed under UHV, STM is capable of achieving atomic resolution in air and in liquid environment, a property which has escalated its use.

More than a decade later, the STM has becomes an instrument for research not only in the field of surface science, but also that of chemistry, biology and medicine. From seeing the atomic structure of a solid surface to molecules adsorbed on a substrate, the STM has indeed becomes a device capable of providing information otherwise impossible to obtain by other experimental techniques.

This thesis presents some STM results of simple organic molecules adsorbed on

solid surfaces. The purpose of this work is to give better understanding of the structural phenomena at the adsorbate/substrate interface, and to address the crucial question in molecular imaging with the STM, namely, the imaging mechanism.

1.2 Principles of Operation

Tunneling, a well known quantum mechanical effect, is the basic principle behind the operation of the STM. The term tunneling describes electrons passing through a region (tunnel junction) in which the potential is such that a classical particle with the same kinetic energy could not pass. Conceptually, consider two closely spaced metal electrodes, as shown in Figure 1.1. When a voltage is applied between the two planar electrodes, electrons are transferred from one metal to the other. This tunneling current (I) for planar electrodes is given by

$$I \propto V \exp (-A\phi^{1/2}s)$$

where V is the applied voltage, ϕ is the average barrier height between the electrodes in eV, s is the separation between the electrodes in Å and A is equal to 1.025 $(eV^{1/2}Å)^{-1}$.

In scanning tunneling microscopy, a sharp tip is placed in proximity to a conducting surface. At this distance, the wavefunctions of the tip and surface overlap. When a bias voltage is applied between the tip and the surface, a quantum mechanical tunneling current begins to flow. The movement of the tip is controlled in three dimensions with an x, y, z piezoelectric element. This voltage sensitive piezoelectric element will bend or deform when an electric field is applied across it. The amount of

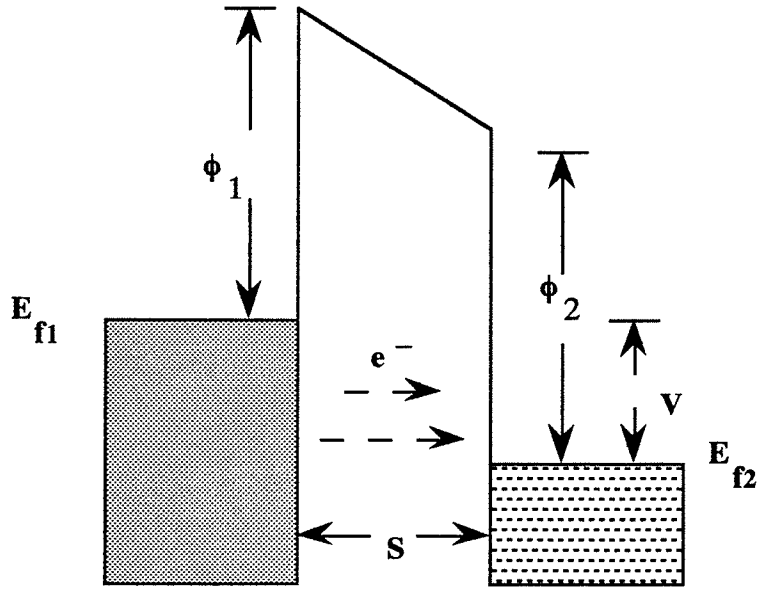

Figure 1.1 Schematic illustration of electron tunneling effect. ϕ_1 and ϕ_2 are the work functions of left and right electrodes, respectively. The voltage *V* opens up a tunneling range so that electrons can move from the left to the right electrode.

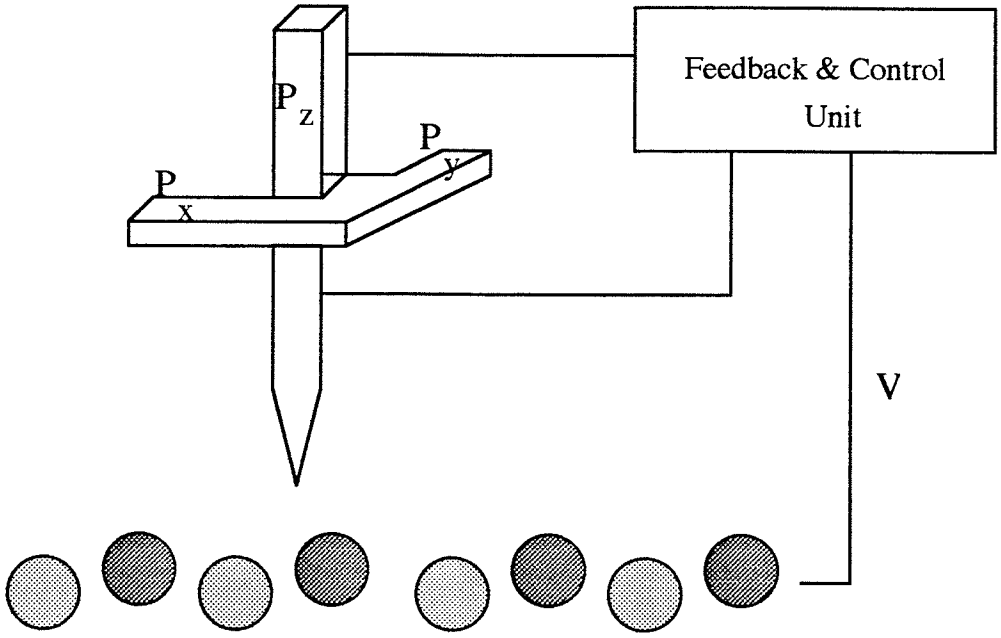

Figure 1.2 A schematic view of the scanning tunneling microscope. Circles represent atoms on surface.

motion can range from atomic to micrometer scale depending on the magnitude of the applied field. Thus a desired area of lateral scan can be achieved by applying the appropriate voltage across the x and y piezo elements. When operating in the constant current mode, while the tip is scanning in the lateral direction, a feedback control system adjusts the voltage to the z piezo, which raises or lowers the tip to keep the tunneling current constant. This adjustment in the z-direction reflects different electronic structures at different sites on the surface or the nature of the surface topography, for example, atomic steps. When the tip is at a location where the tunneling current is high, the z piezo will raise the tip (i.e., increase the tunnel gap) so that constant current is maintained. This gives higher contrast or appears bright in a STM image. Similarly when the tunneling current is low, the tip is lowered, which will result in lower contrast or appears dark in an image. Detailed descriptions of the STM can be found in several review articles [3, 4, 5]. A schematic view of the STM is shown in Figure 1.2. With this instrument, the real space electronic topography of a surface can be imaged to the atomic level.

1.3 Theory

Several representations of the tunneling current have been developed to model how tunneling takes place between the tip and the surface. The widely used theory of the STM is that given by Tersoff and Hamann [6]. Based on the Bardeen formalism [7], where the wavefunctions of the left-right electrodes are treated as separate entities, Tersoff and Hamann calculated the tunneling current using the first order perturbation theory as

$$I = \frac{2\pi e}{\hbar}\sum_{t,s} f(E_t)[1 - f(E_s + eV)]\,|M_{ts}|^2\delta(E_t - E_s)$$

Where $f(E)$ is the Fermi function, V is the applied voltage, E_t is the tip's energy of state Ψ_t in the absence of tunneling, E_s is the surface's energy of state Ψ_s and M_{ts} is the tunneling matrix element between states Ψ_t of the tip and Ψ_s of the surface. M_{ts} is given by

$$M_{ts} = \frac{\hbar^2}{2m}\int d\vec{S}\cdot(\Psi_t^*\vec{\nabla}\Psi_s - \Psi_s\vec{\nabla}\Psi_t^*)$$

where the integral is over the surface lying entirely within the barrier region separating the tip and the surface. Thus the tunneling current arises from the spatial overlapping of tip and surface wavefunctions in the tunnel junction. In the limits of small voltage and low temperature (≤ room temperature), the tunneling current can be written as

$$I = \frac{2\pi e^2 V}{\hbar}\sum_{t,s} |M_{ts}|^2\delta(E_s - E_f)\delta(E_t - E_f)$$

where E_f is the Fermi level of the surface. When the tip is represented by a point probe, the tunneling current is proportional to the surface local density of states (LDOS) at the position of the point probe. Therefore when a STM is imaging in the constant current mode, the image contrast corresponds to the topographical map of the surface LDOS near E_f. The theory is applied to Au(110) surfaces and the results agree well with the experimental values.

1.4 Motivations

The assembly of atoms and molecules on solid surfaces is not only a phenomenon of fundamental interest, but also provides a means to control the chemical phenomena including catalysis, corrosion, lubrication and adhesion. The ability to control interfacial processes are of great scientific and technological interest. It is well established that the STM is capable of imaging a wide variety of atoms, biomolecules, liquid crystals, simple inorganic and organic molecules adsorbed on surfaces. Table I lists some examples in this area of research. However, the imaging mechanism associated with the STM imaging of molecules remains unclear. Most molecules are insulators with large band gaps. When physisorbed on surfaces, one would not expect any electronic contribution from the adsorbed molecules to the tunneling current near the E_f, and thus one would expect that molecules could not be imaged with the STM. There are numerous proposed theories to deal with the question of how molecules are imaged. We will briefly describe a few examples below.

In the imaging of liquid crystals [8], it was proposed that the resulting image contrast observed is due to the local modification of the substrate work function in the presence of the molecules. Adsorbed polar molecules are known to alter the work function of a surface. The adsorbed liquid crystals were proposed to lower the work function of the substrate, thus enhancing the tunneling current and yielding higher image contrast that reflects the positions of the molecules. It was also suggested [9] that the STM actually imaged the molecular orbitals of the liquid crystals.

A recent calculation [10] based on the local density approximation to the density functional theory has shown that weak molecular states of benzene mix with the substrate states of graphite and MoS_2 near the E_f gave images that correspond to the molecular-

substrate interaction. At higher voltage (far away from E_f), the STM imaged the molecular states of the benzene. A similar calculation was performed on a Xe atom physisorbed on a Ni(110) surface [11].

For larger molecules such as the DNA and RNA aggregates, it was proposed that resonant tunneling mechanism is responsible for the success in imaging these molecules [12]. Using the tight-binding model of a molecule in a tunnel gap, calculation showed that the tunneling current increased several orders of magnitude when the molecular states of the biomolecules are in the tunneling range. It was also shown that the pressure in the tunnel gap, which may exceed a GPa, changes the electronic properties of the biomolecules so that the molecular states are near the E_f. Resonant tunneling calculations were also applied to the STM imaging of liquid crystals [13] and other molecules.

G. C. McGonigal et al [14] have studied the adsorption of long chain linear hydrocarbon n-$C_{32}H_{66}$ from solvent onto graphite. The molecules were found to form a highly ordered two-dimensional arrays, as shown in Figure 1.3. Although the STM image reveals striking molecular ordering, the imaging mechanism, however, remains unresolved. Recent ultraviolet photoemission spectroscopy studies of long chain alkanes give the value of the band gap to be about 10 eV, with the lowest-lying unoccupied state just above the vacuum level [15]. It is therefore difficult to understand how these molecules can be imaged with bias voltages not far from the Fermi level, which is located in the middle of the band gap.

It should be noted that the majority of the theoretical calculations were done *after* the STM images had been obtained. To date, there is no general procedure for predicting the image of even a simple molecular monolayer. It may well be that different systems may yield different imaging mechanisms. In order to provide further insight into the

imaging mechanism, it is our intention here to select a simple system such that the imaging mechanism and the structure of the molecular assembly can be carefully examined.

Table I Adsorbate/Substrate Systems Imaged by STM

System	Environment	Reference
Xe on Pt	UHV	16
O on GaAs	UHV	17
Cs on GaAs	UHV	18
S on Re	UHV	19
CO on Rh	Aqueous Solution	20
CO on Pt	Aqueous Solution	21
Naphthalene on Pt	UHV	22, 23
m-CB liquid crystals on graphite	Liquid/Solid Interface	24
Dimethyl and di-2-ethylhexyl Phthalates on graphite	Liquid/Solid Interface	25
Polyimide LB monolayer on graphite	Air	26
Lipid LB bilayers on graphite	Air	27, 28
Polypyrole on graphite and Au	Air	29
Isopolyanion arrays on graphite	Air	30
Detergent monolayer on graphite	Aqueous Solution	31
Glycine on graphite	Glycerol/Water	32
Tosylated β-cyclodextrin on graphite	Air	33
DNA	Air or Water	34 - 36

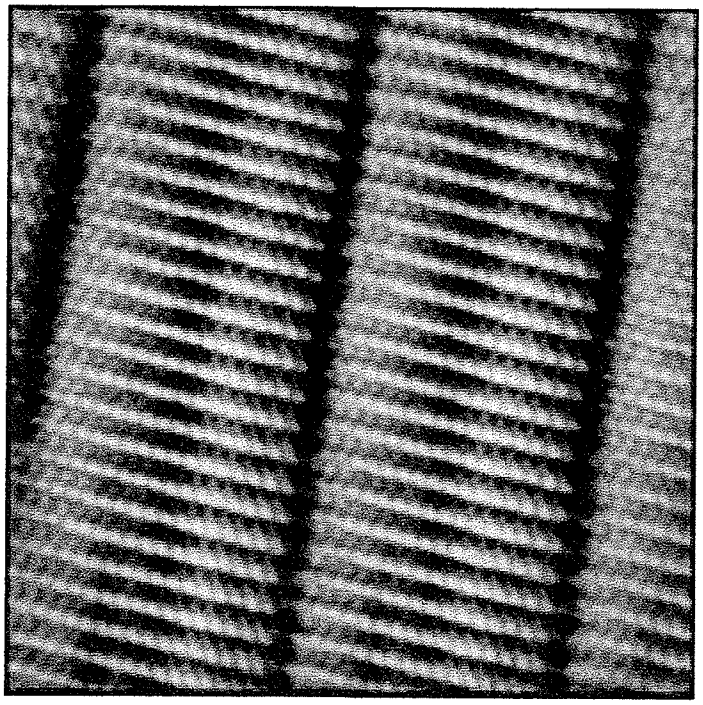

Figure 1.3 Structure of *n*-$C_{32}H_{66}$ observed with STM at solution/graphite interface. Field of view is 100 Å x 100 Å. Bias voltage at 0.4 V and 1.0 nA tunneling current [14].

We have examined three systems with the STM to date. First was the physisorption of *n*-alkanol monolayers at the liquid/graphite interface, where the adsorbed molecules are lying parallel to the substrate. This system has been well characterized by volumetric study. Secondly, we examined the structure of *n*-alkanols and octanoic acid self-assembled at the liquid/Au(111) interface, where the molecules are adsorbed with one end on the surface. Figure 1.4 shows the two adsorption configurations. The adsorbed structures were examined as a function of the bias voltage, substrate temperature and the gap resistance ($R = V/I$, where V is the bias voltage and I is the tunneling current). Some preliminary STM investigations of *n*-alkanes adsorbed on a graphite surface in UHV were also been carried out recently. This is a continuation of the work begun by G. C. McGonigal on the STM of simple organic molecules adsorbed on solid surfaces.

1.5 The Molecules

The *n*-alkanols investigated are *n*-decanol (*n*-$C_{10}H_{21}OH$) and *n*-dodecanol (*n*-$C_{12}H_{25}OH$). Each molecule is a saturated linear hydrocarbon chain with a hydroxyl group at one end, as shown in Figure 1.5. The atoms within the molecules are arranged in a zig-zag chain with C-C and C-O bond lengths of 1.54 Å and 1.44 Å, respectively. Both the C-C-C and C-C-O bond angles are approximately 105.5°. The melting points of the bulk crystal *n*-decanol and *n*-dodecanol are 6.5 °C and 23.9 °C, respectively. Octanoic acid ($C_7H_{15}COOH$) has a similar structure, except that the end of the molecule is an COOH group. The melting point of the bulk crystal of octanoic acid is 16.5 °C. All the chemicals are obtained from the Sigma Chemical Co. and used as received.

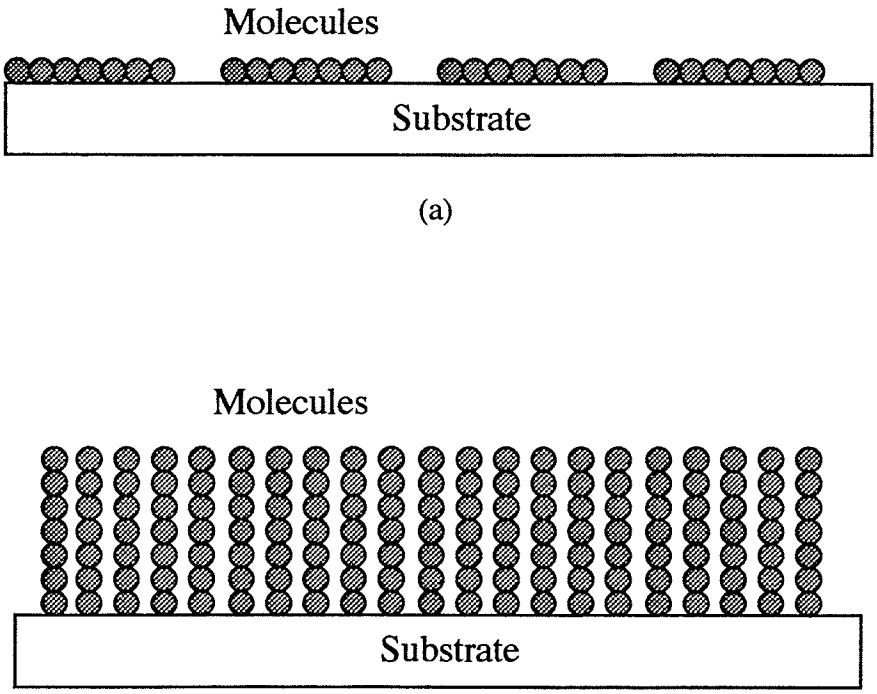

Figure 1.4 Schematic illustration of molecules adsorbed to surfaces (a) parallel and (b) standing on end.

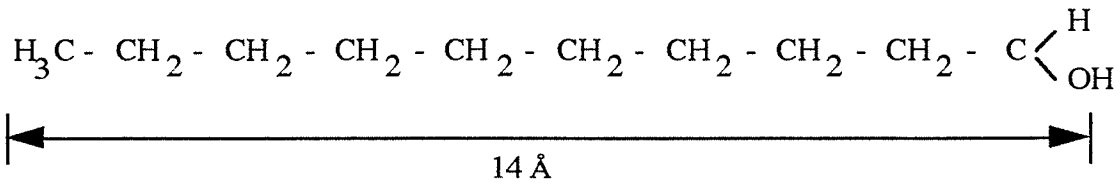

(a) *n*-decanol [*n*-$C_{10}H_{21}OH$]

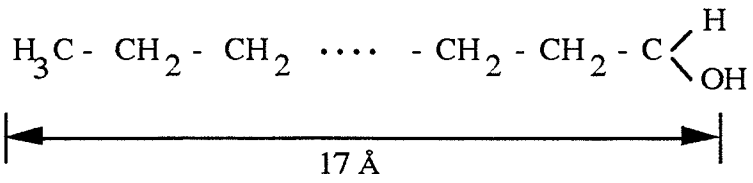

(b) n-dodecanol [*n*-$C_{12}H_{25}OH$]

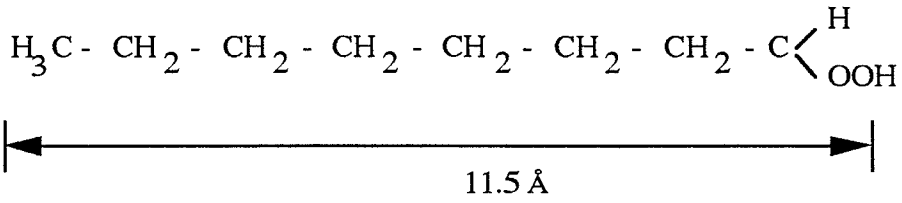

(c) Octanoic acid [$C_7H_{15}COOH$]

Figure 1.5 Schematic drawing of the molecules.

1.6 Experimental Techniques

The research was performed with a Digital Instruments Nanoscope I™ STM. Detailed description of this instrument can be found in reference [37]. The sample was prepared by directly applying the molecules onto a freshly cleaved highly oriented pyrolytic graphite, or onto an epitaxially grown Au(111) film on mica [38]. Because 1-dodecanol has a bulk melting point of 23.9 °C, the temperature of the substrates was raised to produce a liquid/solid environment. This was done by means of a Peltier device situated directly underneath the substrate and the surface temperature was controlled to within ±0.5 °C. The substrate temperature was maintained with the Peltier device throughout the entire experiment. STM images were obtained with a W tip immersed in the liquid and the STM operating on the constant current mode, as shown in Figure 1.6. The W tip was prepared by electrochemically etching in an aqueous solution of KOH (10 gm per 140 ml of distilled H_2O).

1.7 Overview of the Dissertation

The remaining chapters of this thesis deal with the experimental results obtained from the characterization of the adsorbed molecules. Chapter 2 and 3 give the results of STM imaging of the molecules at the liquid/graphite and liquid/Au(111) interfaces respectively. Chapter 4 is devoted to UHV STM imaging of *n*-alkane on graphite. Some general descriptions of the UHV system and the UHV STM will be given. The last chapter deals with the issue of imaging mechanism. We will present some simple calculations to show how the molecules are imaged by the STM.

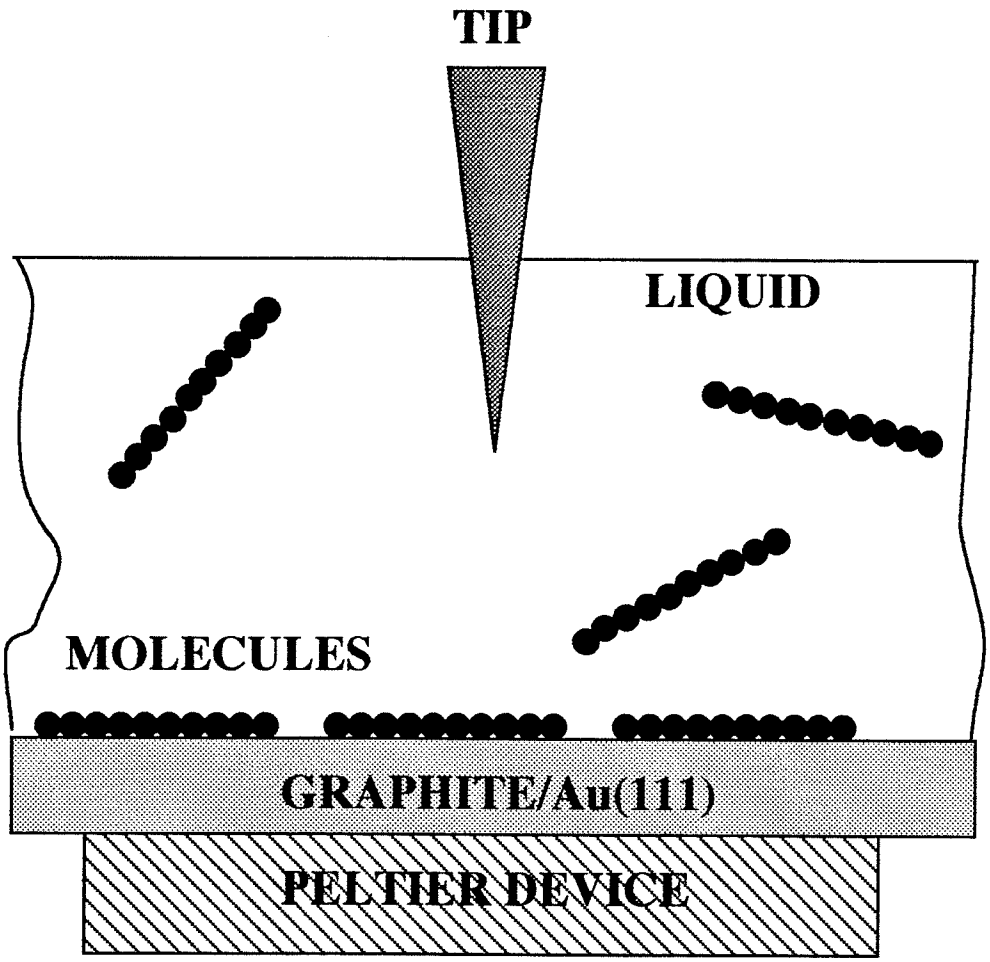

Figure 1.6 STM imaging at the liquid/solid interface.

Chapter 2
Liquid/Graphite Interface

2.1 Introduction

These systems were chosen, in part, because of the previous work on them that could be used as a basis for our work. The presence of ordered *n*-alkanols molecular structure at the liquid/graphite interface has previously been suggested by volumetric and calorimetric studies [39]. The volumetric behaviour of the *n*-decanol and *n*-dodecanol adsorbed on graphite has been studied as a function of temperature [40]. Figure 2.1 shows the result expressed in terms of surface excess mass plotted against the temperature. The region where the surface excess mass is roughly constant corresponds to a monolayer of molecules adsorbed on the graphite surface. For the *n*-decanol, the formation of a monolayer ranges from 10 °C to 45 °C. For the *n*-dodecanol, the formation of a monolayer begins at 28 °C. The disorder transition or melting of the *n*-decanol and *n*-dodecanol ordered structures occur at about 48 °C and 60 °C respectively.

2.2 *n*-Decanol

From previous volumetric studies of *n*-decanol, which suggested the formation of ordered monolayer at the liquid/graphite interface, one could only guess the structure of the adsorbed layer. Figure 2.2 shows an 80 Å x 80 Å STM image of *n*-decanol adsorbed onto graphite. The bias voltage is 0.43 V sample positive and the tunneling current is 0.5 nA. Each molecule is resolved in the STM image. Note that the *n*-decanol monolayer possesses a high degree of two-dimensional ordering. This is the

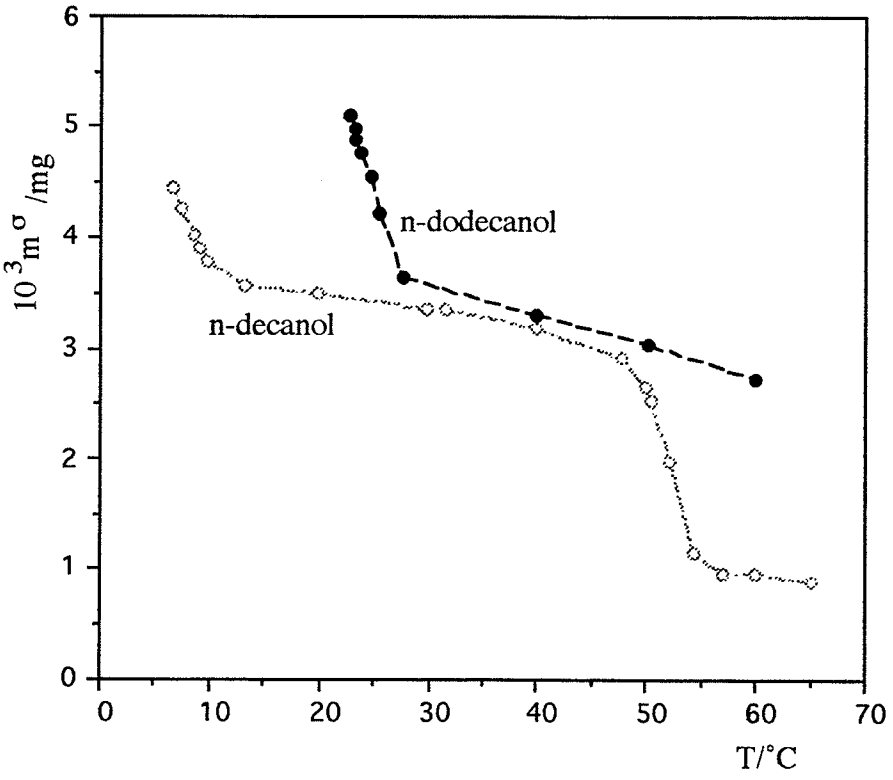

Figure 2.1 Surface excess mass of *n*-alkanols on graphite surface as a function of temperature. Open and solid circles represent *n*-decanol and *n*-dodecanol respectively [40].

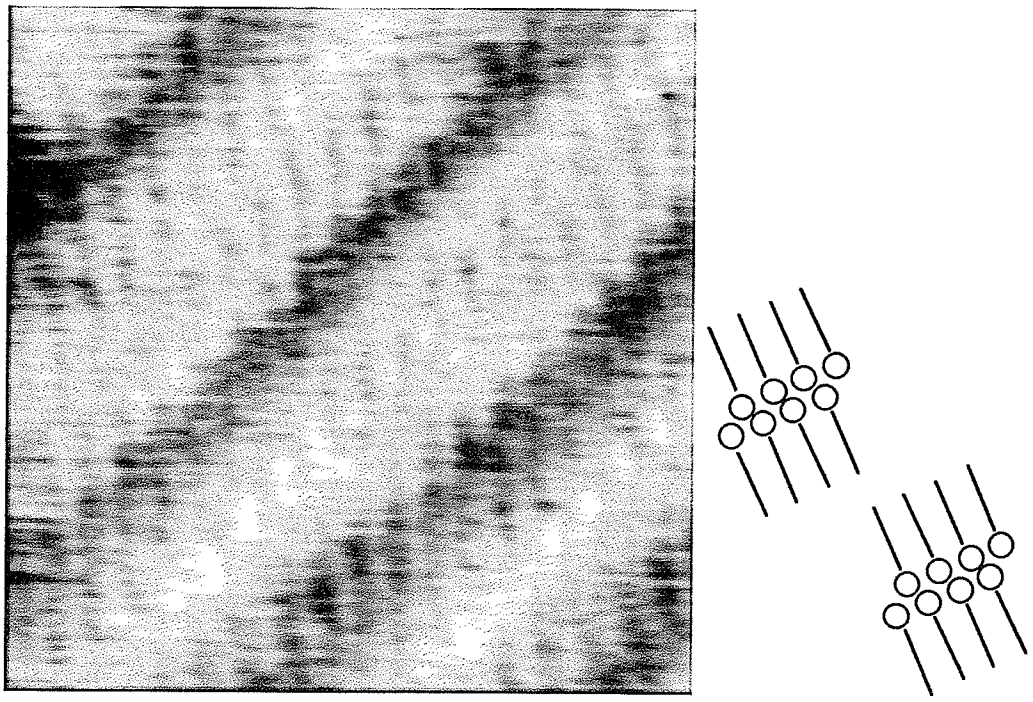

Figure 2.2 (Left) STM image of *n*-decanol on graphite. (Right) molecular arrangement; open circles represent the hydroxyl groups.

first image of *n*-alkanol on graphite revealed by the STM, and shows for the first time the true ordering of the adsorbed layer. The length of each molecule is roughly 14 Å. This is consistent with *n*-decanol lying parallel to the substrate surface. The molecular-packing arrangement of the molecules is such that each bright band consists of molecules linked together in pairs by the hydrogen bonding of the OH head groups in alternate rows. Average separation between two adjacent molecules is approximately 4 Å. The molecules are arranged at an angle of 60^{o} with respect to the dark bands. These features are in agreement with the bulk crystalline form of *n*-alcohols observed from crystallographic analysis [41].

Figure 2.3 shows an image of *n*-decanol taken at 0.1 V bias voltage and 0.66 nA tunneling current. The graphite lattice can clearly be seen, together with narrow 5 Å bright bands. If the bias voltage is raised to 0.33 V while maintaining constant current, higher contrast is achieved and the *n*-decanol monolayer is observed, as shown in Figure 2.4. Comparison between Figures 2.3 and 2.4 suggests that the 5 Å bright bands observed at the 0.1 V bias voltage are associated with the hydroxyl groups within the molecules. On further raising of the bias voltage to 0.45 V, a dramatic change in the STM image contrast occurred as shown in Figure 2.5. The hydroxyl groups now appear as an array of dark holes in the image. The diameter of the hole along the molecular axis is approximately 5 Å, consistent with the width of the bright bands observed at 0.1 V bias voltage. From Figures 2.3, 2.4 and 2.5, we can see that the STM image contrast within the *n*-decanol molecules changes with bias voltage. This voltage-dependent imaging mechanism enables us to selectively image, and therefore identify, the molecule's hydroxyl head group and *n*-alkane tail. To date, the most successful method of locating individual functional groups within a molecule has been the comparison of images of molecules that are identical except for a single functional group [42]. Judicious

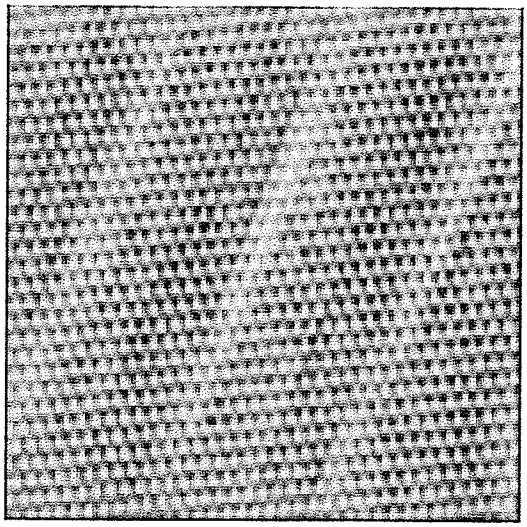

80 Å x 80 Å

Figure 2.3 STM image of *n*-decanol on graphite at 0.1 V.

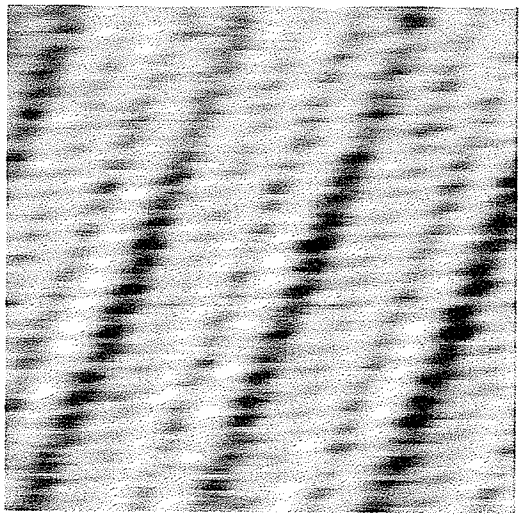

80 Å x 80 Å

Figure 2.4 STM image of *n*-decanol on graphite at 0.33 V.

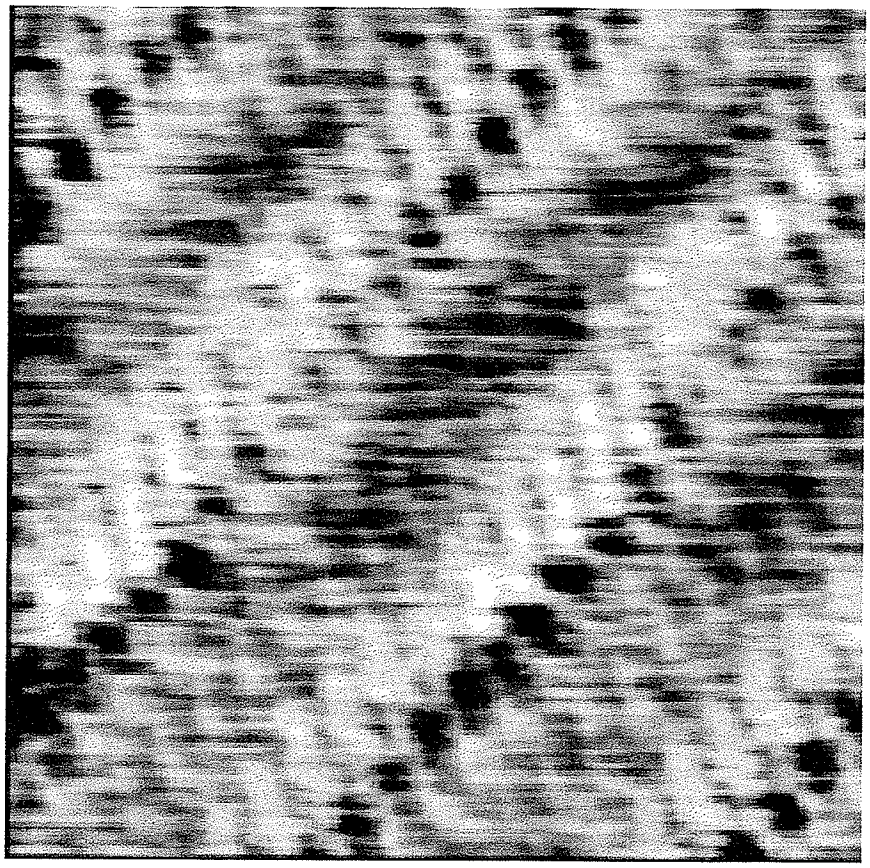

80 Å x 80 Å

Figure 2.5 STM image of *n*-decanol on graphite at 0.45 V.

choice of the substituted functional group yields different apparent heights for that group in each of the STM images, permitting location of the position of the dissimilar functional group in each molecule. Here we have shown for the first time that based on a voltage dependent imaging mechanism, different functional groups within a molecule can be located using the STM.

2.3 Dual-Bias Imaging

To further illustrate the capability of this voltage dependent imaging technique, Figures 2.6(a) and 2.6(b) show images of *n*-decanol and the graphite lattice respectively. These two images are taken simultaneously at two different voltages, while maintaining constant tunneling current. This is done by first completing one scan line at the first voltage, changing the bias voltage, and returning the tip to the start of the line before recording a scan line at the second voltage. The bias voltage is then returned to the first value and the procedure is repeated until two complete images have been obtained. Figure 2.7 shows how the voltage and x-scan change with scan time. From the time interval t_1 to t_2, the line is scanned at voltage V_1 and the data from this scan line is recorded. In returning to the start, which is in between the time t_2 and t_3, the voltage is switched to V_2. The next line is then scanned at voltage V_2 from t_3 to t_4 and recorded. With a typical scan frequency of 20 Hz on 512 lines, the time interval between t_i and t_{i+1} is 0.039 sec.

Figure 2.6(a) displays the two dimensional ordering of the molecules similar to those observed previously. The result confirms that at lower bias, the substrate lattice can be observed without disturbing the adsorbed molecules. In normal imaging, where the graphite lattice and the molecules are separately imaged, the time required to obtain

one image is 25.6 sec. During this time period, thermal drift in the piezoelectric elements can be a big factor if one tries to compare the images of molecules and the graphite to deduce the registry of the adsorbates with respect to the substrate lattice. One image could be offset by a few Å due to the thermal drift and this make comparison of images a difficult task. But with the dual-bias technique, where the molecules and substrate are simultaneously imaged, yields a pair of images offset by no more than the thermal drift occurring during the recording of a single line. Thus this technique can provide a more accurate measurement of the position of the adsorbed simple molecules relative to the substrate. Such technique was also successfully used to simultaneously image a liquid crystal layer and the graphite substrate [43].

(a)

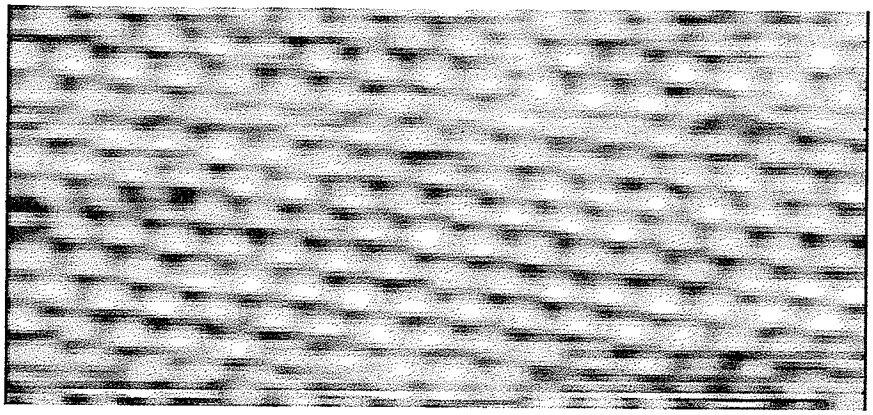

(b)

Figure 2.6 STM images of *n*-decanol acquired simultaneously at bias voltages of (a) 0.48 V and (b) 0.10 V. Field of view is 80 Å x 32 Å.

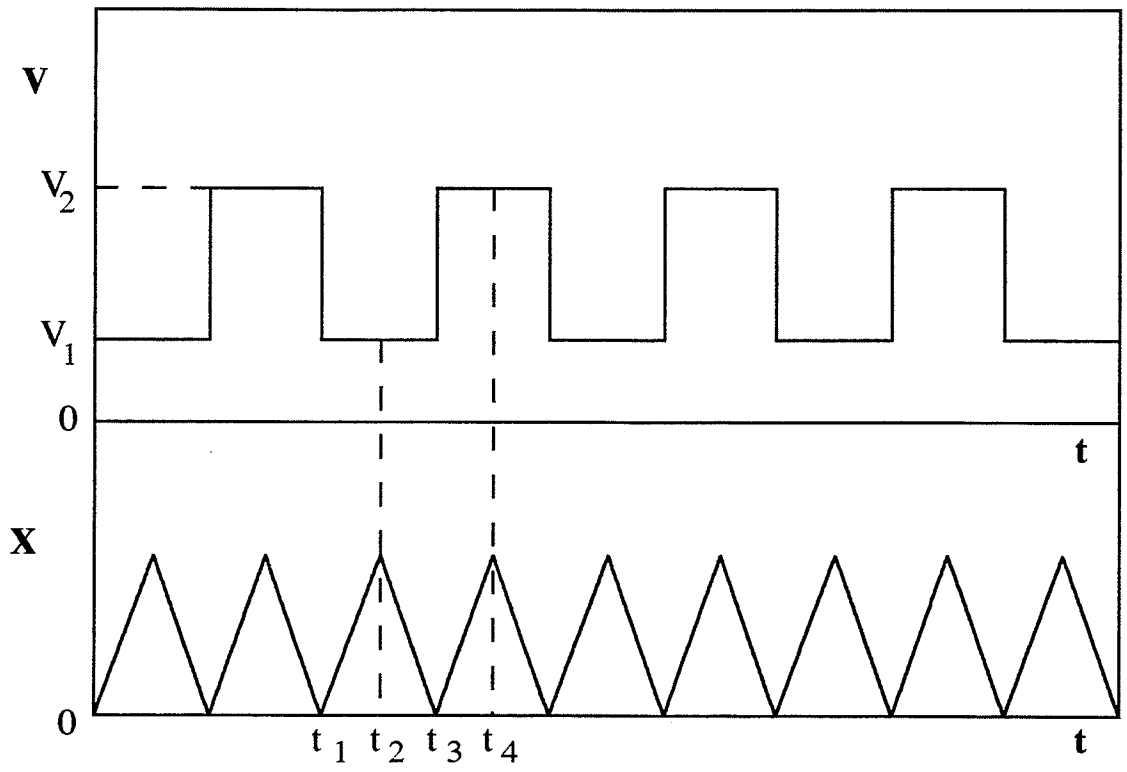

Figure 2.7 Schematic illustration of the procedure for dual-bias imaging.

2.4 The *n*-Dodecanol

Figure 2.8(a) shows an 80 Å x 80 Å STM image of *n*-dodecanol monolayer physisorbed onto the graphite and imaged at 30 °C. The most striking feature observed in this experiment is that the *n*-dodecanol molecules are packed in a herringbone structure (see Figure 2.11(a) for illustration). This structure is quite different from that of *n*-dodecanol bulk crystal [44]. The same structure persists at 35 °C. However, when the temperature of the substrate is raised to 40 °C, a dramatic change in the structure of the adsorbed monolayer takes place, as shown in Figure 2.8(b). While retaining the high degree of two dimensional ordering, the herringbone structure has now transformed into a structure similar to the bulk crystal, and similar to that observed for *n*-decanol on graphite. Although it was believed from the volumetric studies that this interfacial structure was ordered, it was not suspected however that there was on order-order phase transition between the bulk melting temperature and the melting temperature of the interfacial layer (or disorder transition). For the first time the STM has revealed the behaviour of this ordered structure.

The long range ordering of the adsorbed molecules at the two temperatures are shown in Figures 2.9(a) and (b). At 30 °C, we observed a moiré pattern of alternating high and low contrast repeated on a length scale much larger than the molecular size, which is different from that at 40 °C. We believe that the moiré pattern results from neighboring molecules adsorbed at slightly different substrate sites. A simple illustration on the origin of the moiré pattern is shown in Figure 2.10. Figure 2.10(a) shows an adsorbed layer of atoms (shaded circles) binding at equivalent sites on the substrate (open circles). This corresponds to a commensurate structure. Therefore the STM contrast of the adsorbed atoms should be the same. In Figure 2.10(b), where the atoms are

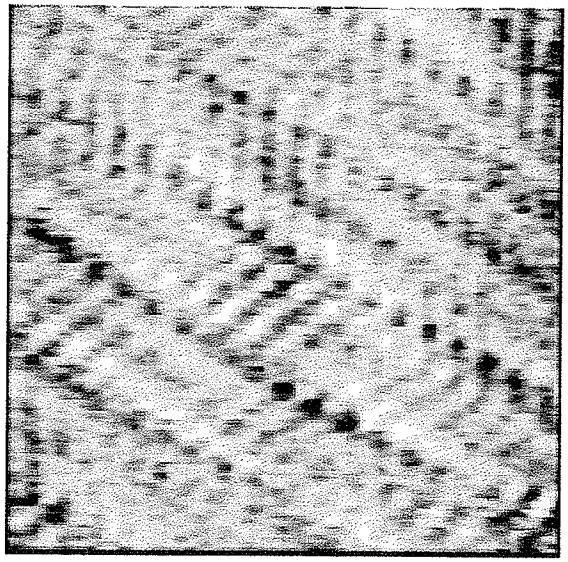

(a)

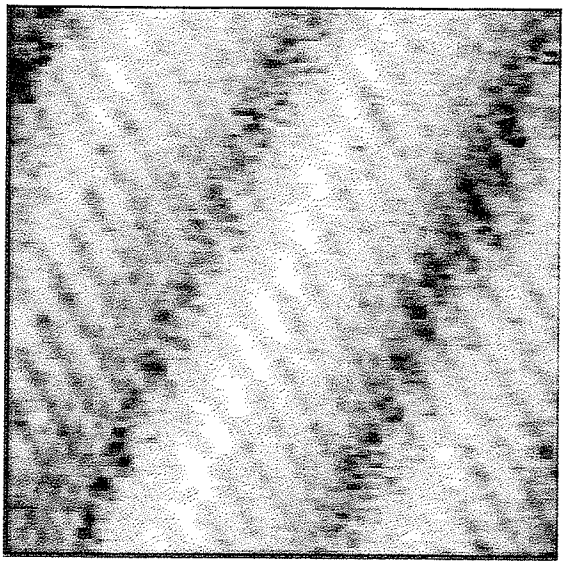

(b)

Figure 2.8 STM image of *n*-dodecanol on graphite at two temperatures (a) 30 °C and (b) 40 °C. Image size is 80 Å x 80 Å.

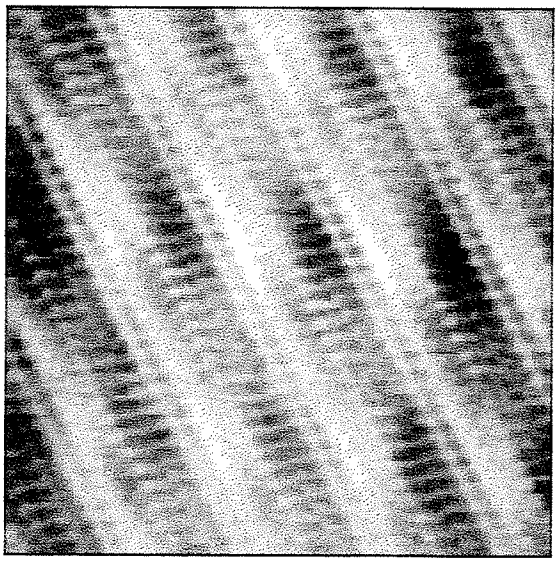

(a)

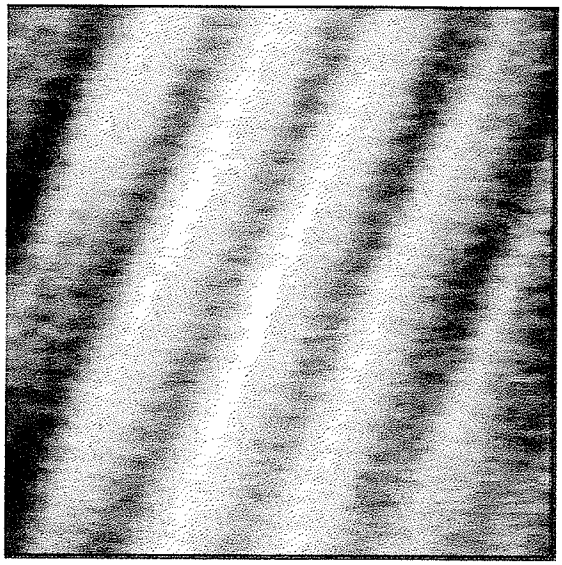

(b)

Figure 2.9 Long range ordering of *n*-dodecanol on graphite (a) 30 °C and (b) 40 °C. Image size is 160 Å x 160 Å.

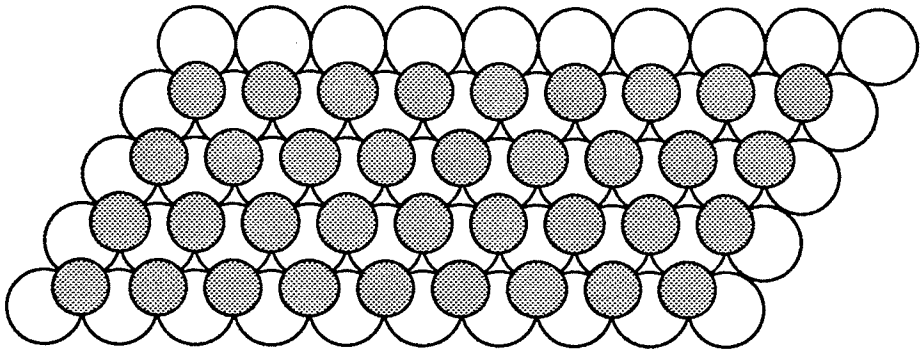

(a)

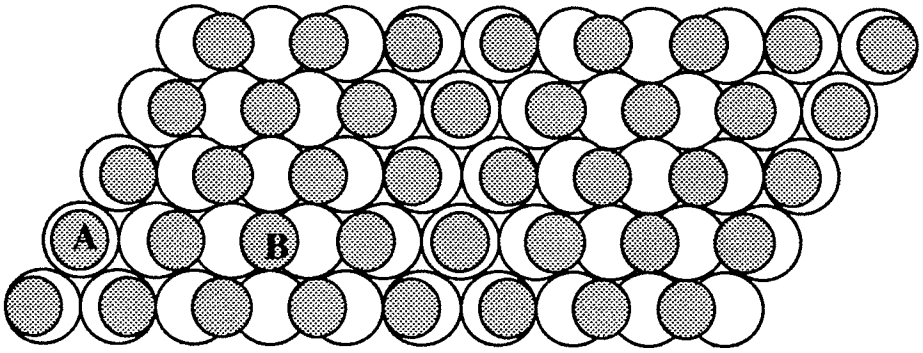

(b)

Figure 2.10 Illustrations of (a) commensurate and (b) incommensurate structures. (b) gives rise to moiré pattern in an STM image. Open and shaded circles represent the substrate and adsorbed atoms respectively.

adsorbed at inequivalent sites on the substrate, this is referred as an incommensurate structure. The adsorbed atom *A* will appear brighter than atom *B* in an STM image as it is on top of an substrate atom; while atom *B* is situated in between two substrate atoms. This high and low contrast will show up as moiré pattern when the long range ordering of the adsorbed layer is imaged. We can infer that in the imaging of *n*-dodecanol, the molecular monolayer may be incommensurate with the substrate lattice at 30 °C; while a commensurate structure is possible at 40 °C.

It is possible the structural phase transition of *n*-dodecanol observed is due to the presence of rotator phases at higher temperature. The rotator phase has previously been observed in the x-ray studies of Langmuir monolayers and solid *n*-alkanols [45, 46]. In a rotator phase the alkane tails rotate about their axis. Figures 2.11(a) and (b) show schematic representations of the two types of *n*-dodecanol ordered structures observed. Intermolecular spacings measured along the *a*-axis at 30 °C and 40 °C are approximately 4.8 Å and 6.2 Å respectively. The increase in the intermolecular spacing is consistent with the existence of rotational mode at the higher temperature. At 40 °C, the molecules could rotate about their C-O axes due to the increase in thermal energy and the effect of this rotational mode transforms the *n*-dodecanol monolayer structure from herringbone to a structure similar to that of the bulk crystal.

It is important to note that the herringbone structure reappears when the substrate temperature is lowered from 40 to 30 °C. In other words, we do not observe any hysteresis in this transition. Also, we do not observe any adsorbed monolayer above 45 °C. This could due to the instability of the monolayer at higher temperature. It has been suggested that in the ethanol/graphite system [47], the melting of the ethanol monolayer takes place via a two-step mechanism. First is the melting of the alkyl tails, while the hydrogen bonds are maintained and ensure the stability of the monolayer. Second, at

sufficiently high temperature, the hydrogen bonds break and an order-disorder transition occurs. Figure 2.12 illustrates the melting behaviour of the ethanol/graphite system. When the temperature is raised, the molecules undergo rotations about their C-O axes prior to the breaking of the hydrogen bonds. Our results also indicate such a step-wise nature of increased disorder, with alkyl tail transitions occurring at lower temperature. This provides a further insight into the behaviour of two-dimensional system processes such as order-order transition and 'two-dimensional melting'.

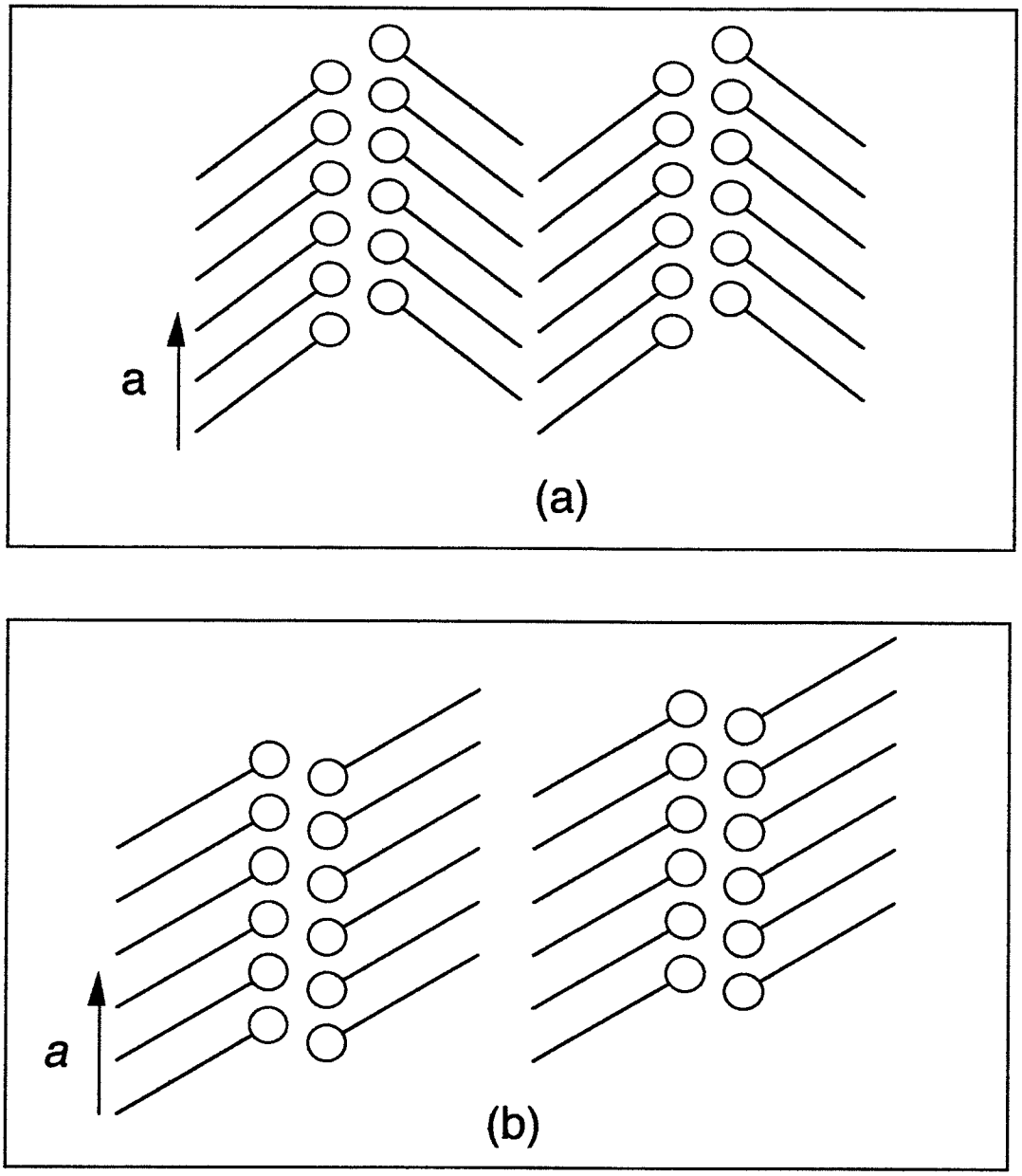

Figure 2.11 Schematic representation on the structures of *n*-dodecanol monolayer physisorbed on graphite at (a) 30 °C and (b) 40 °C. Open circles are the OH head groups.

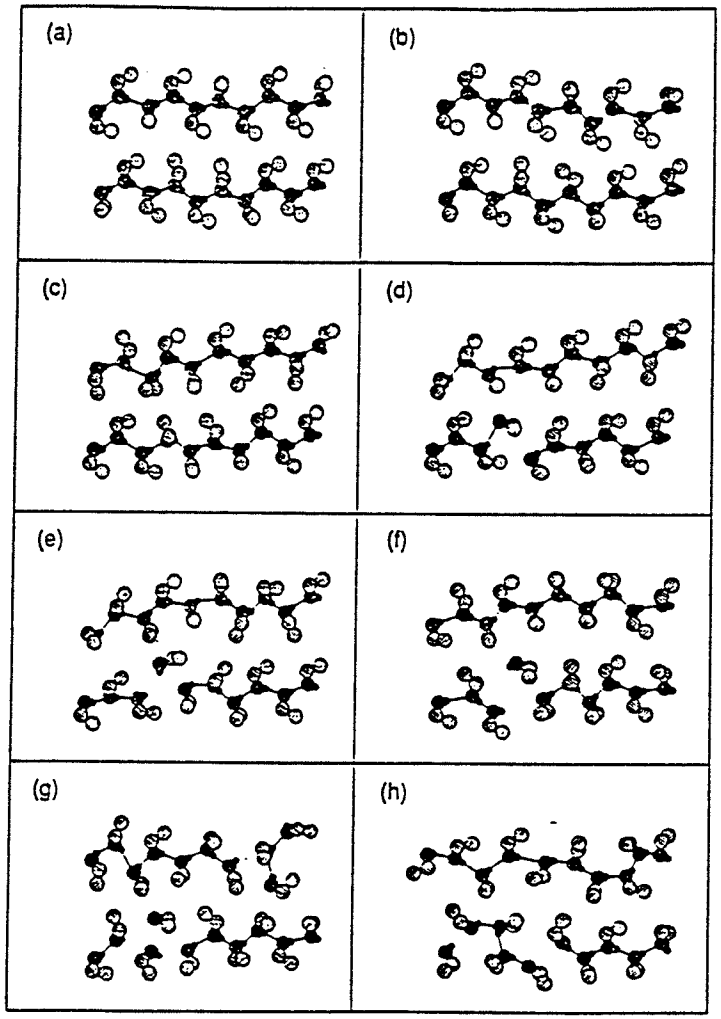

Figure 2.12 A schematic view from above the surface of the melting of physisorbed ethanol. Black circles are the oxygen atoms. Shaded circles are the carbon atoms of the hydrocarbon chains. Hydrogen bonds are illustrated by solid lines. Circles which obscure other circles indicate atoms farther from the surface. The temperature increases in successive frames [47].

Chapter 3
Liquid/Au(111) Interface

3.1 Introduction

The behavior of self-assembled molecular monolayers on surfaces has been the subject of active scientific investigation [48]. Detailed understanding of molecular organization in two dimensions is important to the engineering of materials at the molecular level. Recent work by G. M. Whitesides [49] demonstrates the potential of performing lithography in the molecular scale using these molecular assemblies. A traditional system for studying self-assembled monolayer has been the adsorption of *n*-alkanethiols $[CH_3(CH_2)_nSH]$ on gold surfaces [50]. The self-assembly of *n*-alkanethiols on Au(111) was recently investigated with the STM [51]. For *n*-alkanols adsorbed on other metal surfaces, electron diffraction studies proved that ordered monolayers were formed with their hydrocarbon tails perpendicular to the substrate [52]. The search for ordered *n*-alkanols on a gold surfaces has been unsuccessful in the past. Although the *n*-alkanethiols bind more strongly than *n*-alkanols on a gold surface [53], contrary to popular belief the *n*-alkanols can also form an ordered self-assembled layer at the liquid/Au interface, as demonstrated by out STM measurements. In the following, we provide the first observation of ordered *n*-alkanol molecules self-assembled at the liquid/Au(111) interface with the STM. Our results show striking similarity between the self-assembled of *n*-alkanethiols and *n*-alkanols on Au(111).

3.2 *n*-Decanol

The Au(111) film was prepared by evaporation onto a heated mica substrate in vacuum. The substrate temperature was 450 °C. After the evaporation, the film was kept in the vacuum system at the same temperature and annealed. Sample preparation procedure for the STM experiment is similar to that of the liquid/graphite interface. Few drops of *n*-decanols were placed directly onto the Au(111) film. The STM images were obtained with an electrochemically etched W-tip immersed in the liquid. Figure 3.1 shows a 40 Å x 40 Å STM image of the Au(111) substrate obtained at the *n*-decanol/Au(111) interface under ambient conditions. The bias voltage is 0.5 V sample positive and the tunneling current is 0.5 nA [54]. Atomic resolution of this image gives a nearest-neighbour spacing of 3 Å, consistent with that observed in ultra-high vacuum STM imaging of Au(111) [55]. It was found that a threshold bias of 0.5 V must be exceeded before the *n*-decanol monolayer is observed, below this threshold the gold substrate is revealed. There was no evidence of the presence of the monolayer when the STM was operating at opposite tip polarity (sample negative), even at higher voltages.

By raising the bias voltage, the STM image contrast changes and the *n*-decanol adlayer was observed. Figure 3.2(a) shows a 60 Å x 60 Å STM image of *n*-decanol adsorbed on the Au(111) surface. The bias is 0.57 V sample positive and the tunneling current is 0.66 nA. Clearly observable is a hexagonally close-packed array with a nearest-neighbour spacing measured to be approximately 5 Å. This spacing agrees well with the expected diameter of a hydrocarbon chain. We believe this to be an image of the *n*-decanol molecules standing on end with the OH polar groups facing the gold substrate [56]. The bright dots would then correspond to the methyl groups at the end of the hydrocarbon chain. The hexagonal close-packing, and the corresponding interchain

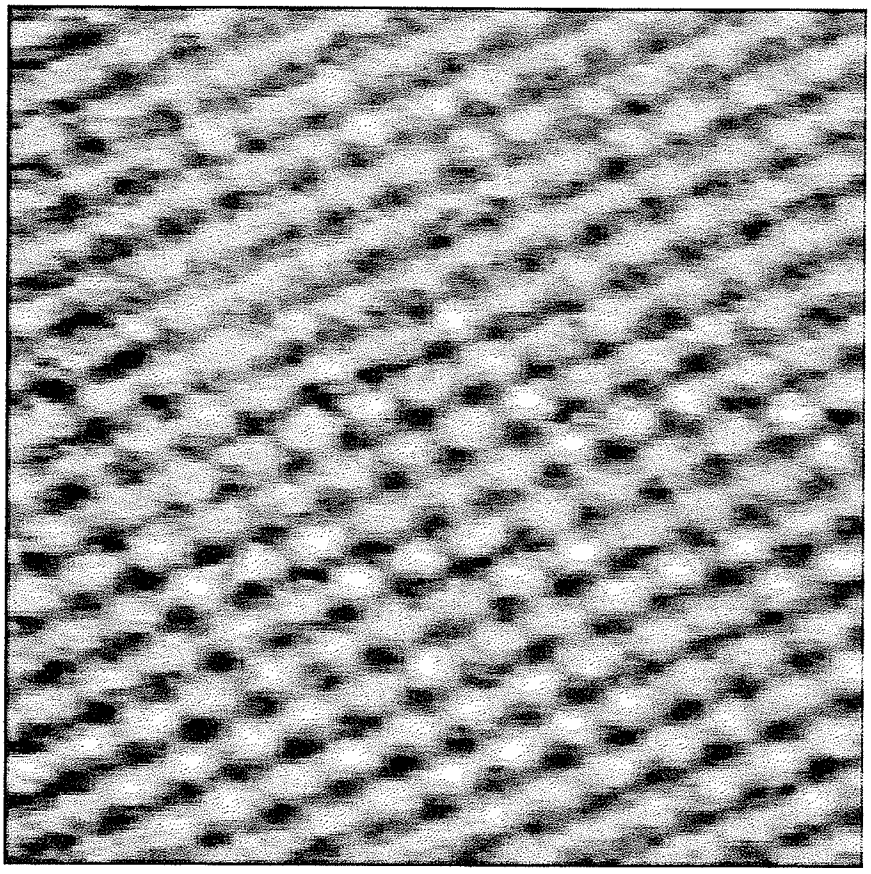

40 Å x 40 Å

Figure 3.1 STM image of an epitaxially grown Au(111) surface in liquid *n*-decanol environment.

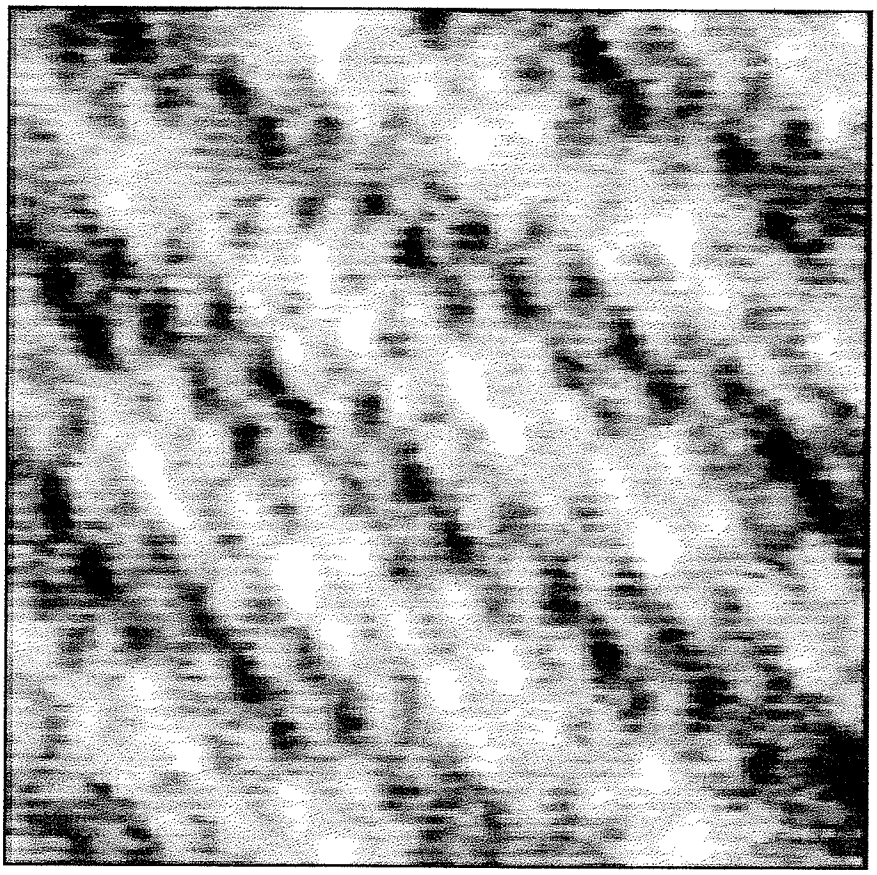

60 Å x 60 Å

Figure 3.2(a) STM image of *n*-decanol self-assembled at the liquid/Au(111) interface.

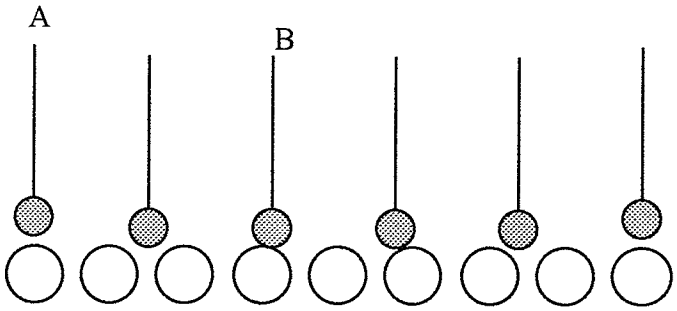

Figure 3.2(b) Schematic illustration of the contrast observed. Position *A* gives higher contrast than *B*. Open circles represent the Au lattices.

spacing are similar to the packing arrangement of docosyl mercaptan [$CH_3(CH_2)_9SH$] on Au(111) observed from electron and helium diffraction studies [57, 58]. Note that the image also reveals a superstructure pattern of alternating areas of high and low contrast. This moiré effect is consistent with the OH head groups binding at inequivalent sites, thus yielding higher contrast at different locations on the gold surface, as illustrated in Figure 3.2(b). It is interesting to note that a recent helium diffraction study of *n*-octadecanethiol on Au(111) also showed the formation of superlattice structure [59]. Two-dimensional Fourier analysis of Figure 3.2 shows that both the underlying adlayer and the superstructure exhibit hexagonal patterns.

3.3 *n*-Dodecanol

To investigate further the adsorption of *n*-alkanols on Au(111), we imaged the *n*-dodecanol molecules. Figure 3.3 shows an image of *n*-dodecanol at the liquid/Au(111) interface. The 80 Å x 80 Å image is taken at 770 mV and 0.35 nA, which corresponds to a gap resistance of 2.2 GΩ. The image reveals a hexagonal superstructure pattern of alternating areas of high and low contrast. Although we cannot resolve the nearest neighbour spacing of the molecules, the superlattice structure observed here is similar to our previous STM results of *n*-decanol on gold, which clearly showed the 5 Å intermolecular spacing.

We found that the STM image obtained in the experiment varies strongly with the gap resistance of the tunnel junction. In Figure 3.4, the STM image is taken with 0.12 GΩ gap resistance. This 60 Å x 45 Å image shows a series of squares with a periodicity of approximately 5.2 Å (distance between center of squares). It appears that this image corresponds to a reconstructed Au(111) surface in the presence of the molecules. Each square consists of 8 Au atoms covering an area of 30 $Å^2$. This gives the nearest neighbor

separation between the Au atoms along the sides of the square to be approximately 2.7 Å. Figure 3.5 shows an image with 0.16 GΩ gap resistance. The square pattern is maintained but somewhat disordered. This suggests that the reconstructed Au(111) surface is unstable, and can be manipulated by changing the gap resistance of the tunnel junction. Figure 3.6 shows an image across three terraces on the gold surface. The square pattern is visible on two terraces, which shows that the origin of this pattern is not due to some anomalous tip effects that might occurred in the tunneling experiment. The gap resistance in this image is 0.29 GΩ.

The formation of square pattern on a reconstructed Au(111) surface is by no mean restricted to STM imaging *n*-dodecanol at the liquid/solid interface. Recent STM studies of gold exposed to sulfide, thiocynnate and *n*-octadecanethiol also yield similar results [60, 61]. It was proposed that under specific imaging parameters, the *n*-octadecanethiol molecules are removed from the surface, along with the Au atoms that are attached to the sulphur head groups. The result is the reconstruction of Au(111) surface into a series of squares. In the case of imaging *n*-dodecanol molecules, the STM image varies with the gap resistance. It demonstrates that at higher gap resistance (i.e. large tunnel junction), the STM image displays those of the adsorbates. Decreasing the gap resistance removed the adsorbates from the gold substrate by the STM tip. Although the OH head groups of *n*-dodecanol bind less strongly to the substrate than the SH head groups of *n*-octadecanethiol molecules, there is the possibility that Au atoms were removed from the surface together with the molecules, for the resulting square pattern is similar to that in imaging *n*-octadecanethiols.

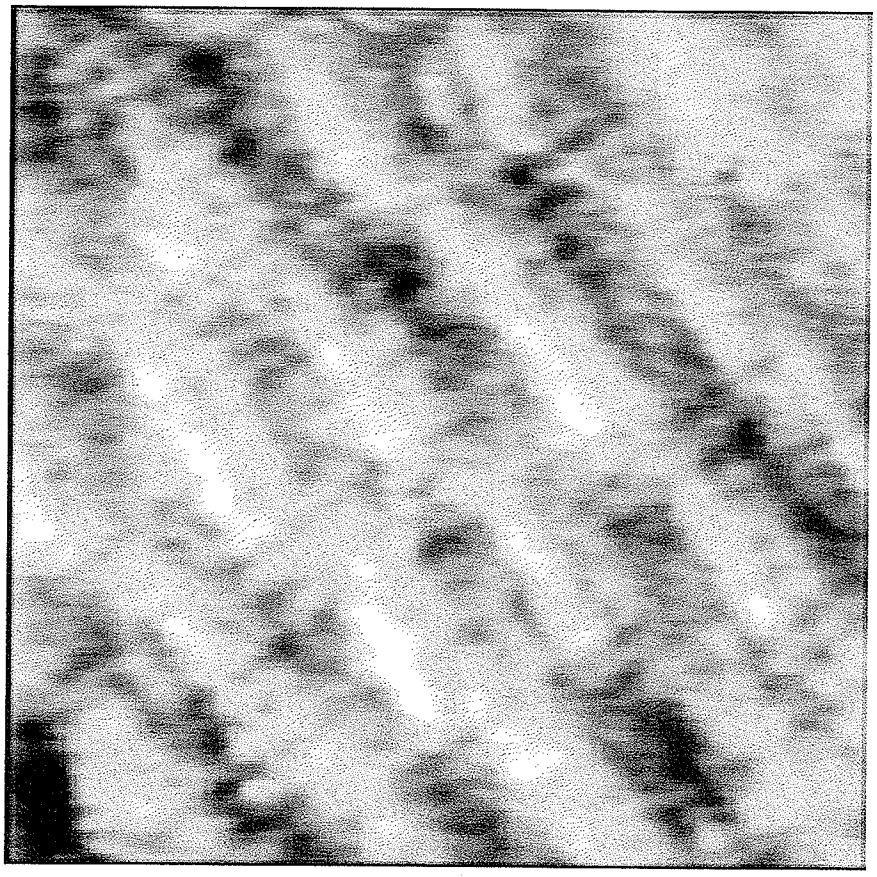

80 Å x 80 Å

Figure 3.3 STM image of *n*-dodecanol self-assembled at the liquid/Au(111) interface.

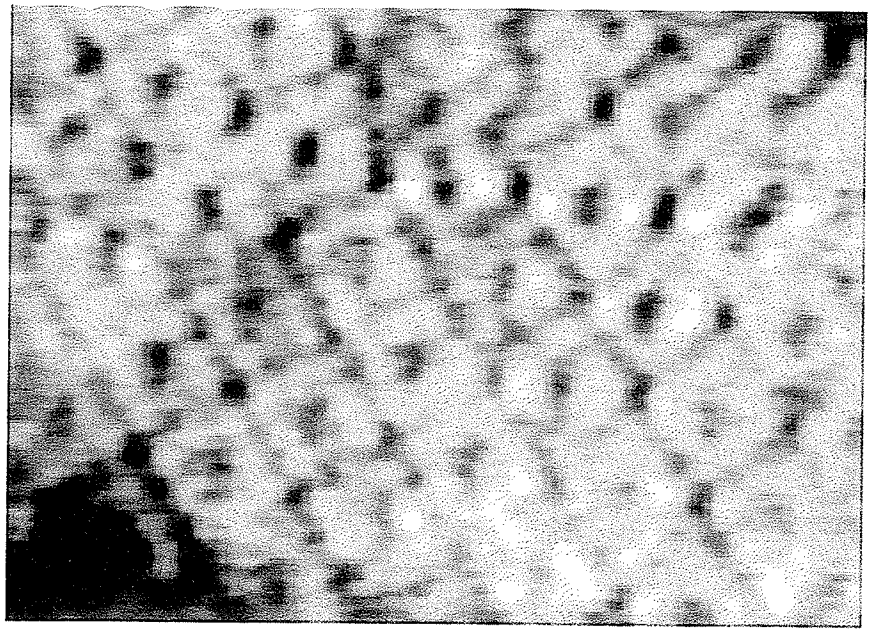

60 Å x 45 Å

Figure 3.4(a) Image of reconstructed Au(111) when gap resistance is reduced to 0.12 GΩ. This square pattern is imaged at 100 mV and 0.8 nA.

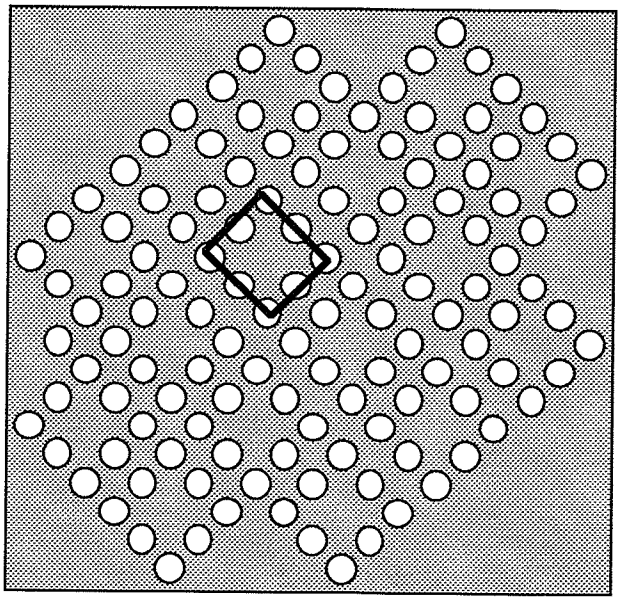

Figure 3.4(b) Drawing of the square pattern. Each square consists of eight Au atoms.

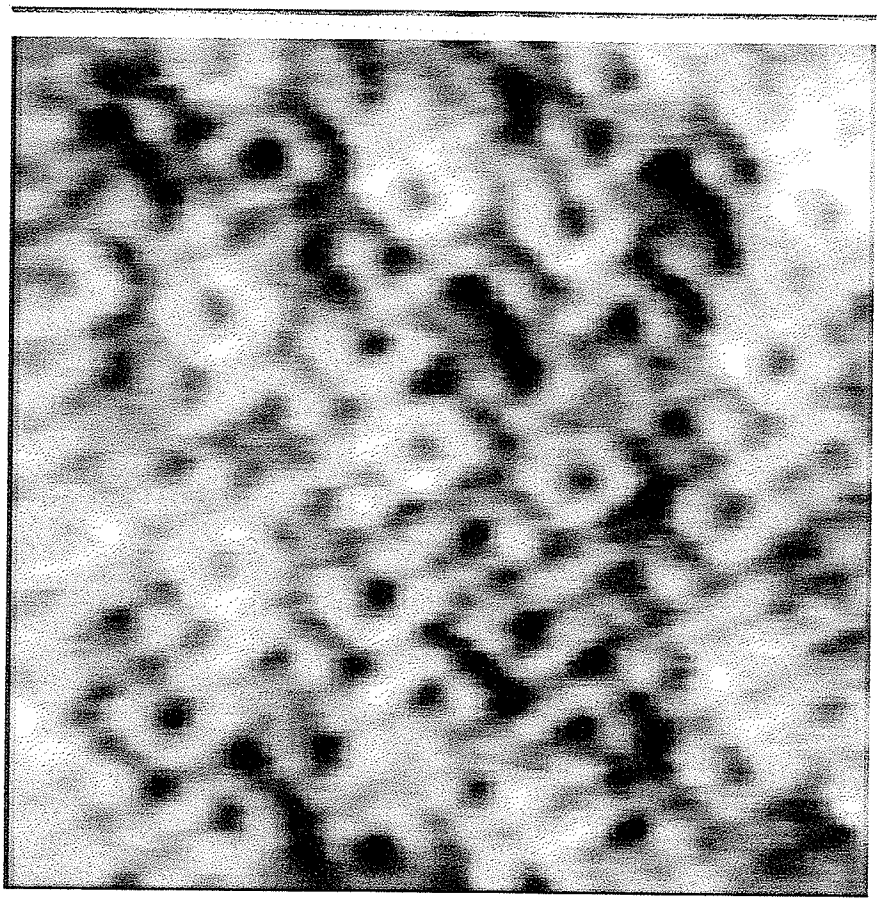

Figure 3.5 Disordered square pattern at 0.16 GΩ. Image size is 60 Å x 60 Å.

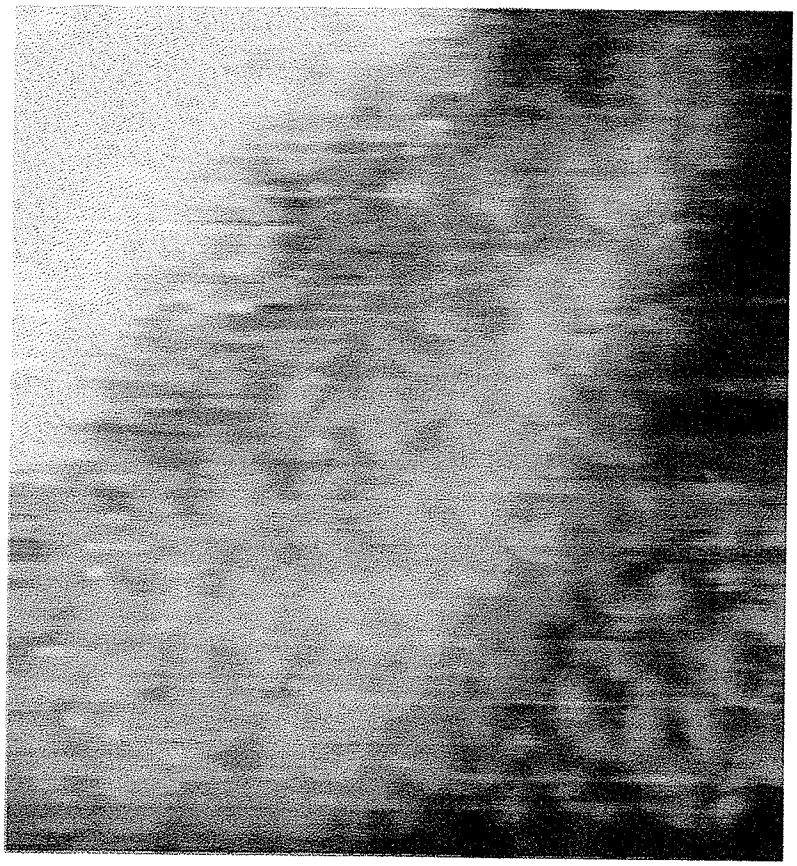

Figure 3.6 55 Å x 60 Å image of square pattern across two gold terraces.

3.4 Octanoic Acid

The adsorption of *n*-alkanoic acids on metals such as Al, Ag, and Cu has been well characterized [62]. There has been no account of a corresponding monolayer on Au. Figure 3.7 shows a 60 Å x 60 Å image of octanoic acid adsorbed at the liquid/Au(111) interface. The image is taken with a gap resistance of 1.86 GΩ. A close-packed array of dots can be seen from this image. The nearest-neighbour spacing between dots is approximately 5 Å. This is consistent with the diameter of the molecules when adsorbed with their hydrocarbon chains pointing outward from the surface. A recent study of long chains alkanoic acids adsorbed on silver indicated that the molecules were oriented normal to the surface [63]. Also observable in this image is the superlattice structure. This moiré pattern could be due to the COOH head groups binding at different sites on the surface, as in the case of *n*-decanol and *n*-dodecanol. Fourier transform of this image shows both the underlying lattice and the superstructure exhibit hexagonal pattern. When the gap resistance is decreased, the STM image becomes disordered. Further decrease in the gap resistance gives the image of Au(111). We are not able to observe any reconstruction of the gold surface in imaging octanoic acid. This does not means that the reconstruction of the surface could not take place when imaging octanoic acid. As we have shown in the imaging of *n*-dodecanol, there exists only a narrow range of gap resistance at which the unstable reconstructed surface can be imaged.

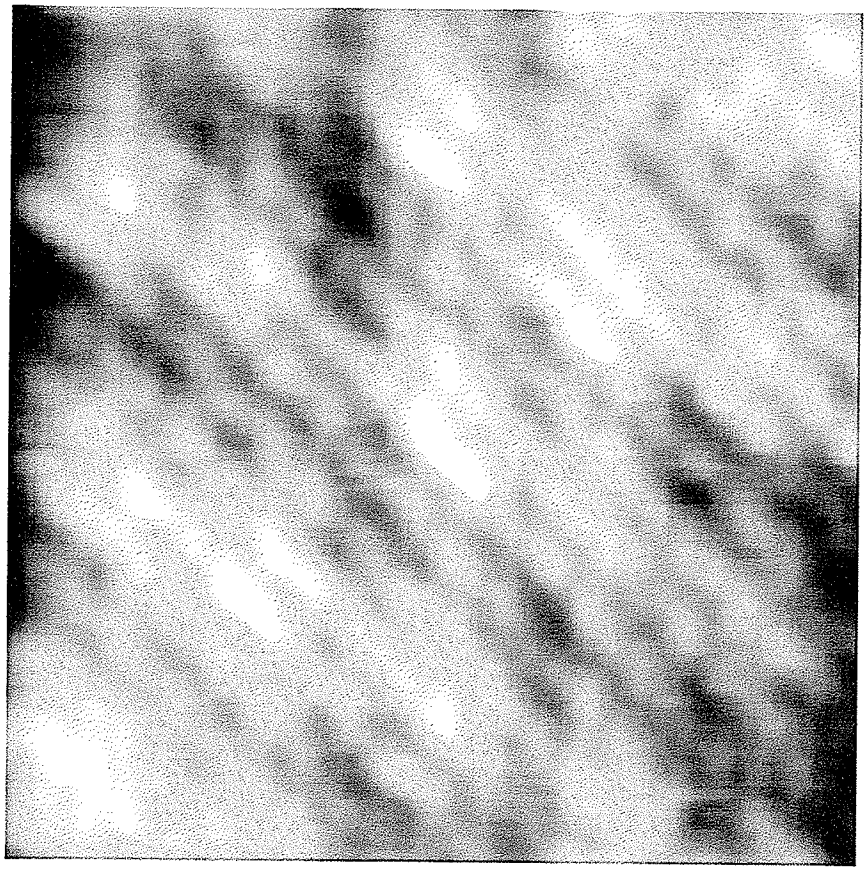

60 Å x 60 Å

Figure 3.7 Image of octanoic acid on Au(111) taken at 0.67 V and 0.36 nA.

Chapter 4

UHV Imaging of *n*-Alkane

4.1 Introduction

In chapter 2 and 3, we have demonstrated that the STM can provide detailed structural information of adsorbates at the liquid/solid interfaces. In order to get a better understanding of the imaging mechanism, we need to perform experiments in an UHV environment where the conditions are better controlled. Unfortunately, experiments at the liquid/solid interface are not well controlled. It is difficult to determine the role of the fluid in the imaging mechanism. UHV imaging of atoms and molecules on solid surfaces has been successful in the past. Examples include the imaging of Xe atoms on Ni(110) [11] and benzene coadsorbed with CO molecules on Rh(111) [64], showing ringlike structures which corresponding to the benzene molecules. Larger molecules such as the duplex DNA on graphite were also observed in UHV and the images revealed the two helical turns of the biomolecule [65]. In the case of imaging long chain *n*-alkanes on graphite, all the experimental results were obtained from liquid/graphite environment.[66, 67]. The long chain linear hydrocarbon *n*-alkanes were found to physisorb from solvent onto the graphite in a highly ordered two dimensional array. No data on the STM imaging of these molecules in UHV are available to date.

Shorter *n*-alkanes such as *n*-hexane (*n*-C_6H_{14}) molecules are known from neutron diffraction studies to form ordered structures on graphite in UHV at temperatures below 150 K [68]. To examine the formation of *n*-alkane ordered structures at room temperature however, longer chain molecules are needed. To find out whether these long chain *n*-alkanes are stable when adsorbed on graphite at room temperature, we estimated

the surface mobility of the molecules by using the diffusion equation [69]

$$D = D_o \exp(-E_d / KT)$$

where D is the diffusion coefficient, D_o is the pre-exponential factor and is of the order of 10^{-3} cm^2/s. E_d is the surface diffusion activation energy, K and T are the Boltzmann constant and temperature respectively. Figure 4.1 shows a schematic diagram of energy versus position on a surface. For a molecule to jump laterally from one well to another, it has to overcome the barrier E_d. For a n-$C_{26}H_{54}$ molecule, the binding energy is approximately 2.5 eV when adsorbed on graphite [70] and E_d is typically 30 % of the binding energy [71]. Therefore at room temperature, D is approximately 3 x 10^{-16} cm^2/s. In a time interval of t = 1 sec, the molecule moves $x = (Dt)^{1/2} \approx 2$ Å. In the present UHV experiment, the time required to complete an image is 512 sec. An isolated molecule therefore cannot be imaged due to the mobility of the molecule. If the molecules formed an ordered structure, this structure could be stabilized due to the lateral interactions between the adsorbed molecules and would be possible to image with the STM. The diffusion coefficient D can be reduced by choosing molecules with chain length longer than that of n-$C_{26}H_{54}$; but the vapor pressures of these molecules are much lower than a typical UHV environment (10^{-10} torr), rendering the sample preparation procedure difficult. In this chapter, a preliminary *in situ* UHV STM study of the n-alkane molecules, in particular the n-$C_{26}H_{54}$ adsorbed on graphite will be presented.

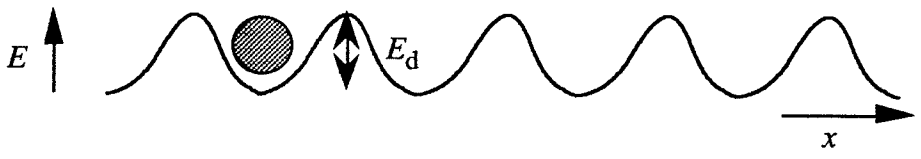

Figure 4.1 Schematic illustration of energy barrier on a surface. Shaded circle represents an adsorbate on the surface.

4.2 Instrumentation

Figure 4.2(a) shows the UHV system. A Park Scientific™ UHV STM-SU2 is placed in the chamber, to be used in conjunction with a low energy electron diffraction (LEED) instrument. Surface characterization of the graphite and adsorbates on substrate is performed with LEED prior to STM imaging. Approximately 10 mg of the *n*-$C_{26}H_{54}$ molecules are placed in a glass tube and isolated with a gate valve in a differentially pumped sublimation port, as shown in Figure 4.2(b). This allows LEED to be performed on a clean graphite surface without the contamination of the *n*-$C_{26}H_{54}$ molecules. The vapor pressure of some long chain *n*-alkanes as a function temperature is plotted in Figure 4.3. For the *n*-$C_{26}H_{54}$ molecules, the vapor pressure is approximately 5×10^{-7} torr at room temperature. The pressure in the port is maintained at 1×10^{-8} torr.

A schematic drawing of the UHV STM is shown in Figure 4.4(a) and (b). Vibration isolation of the inner stage is achieved by using a double spring suspension along with magnetic damping. The inner stage is suspended from the middle stage, which in turn is suspended from the outer frame of the entire instrument. The W tips are prepared in air, the same way as described earlier. A maximum of eight tips can be put in the tip carousel, located near the inner stage. This makes *in situ* tip replacement possible, without having to vent the vacuum system everytime a tip is replaced. The tip scanner is formed by configuring three piezoelectric bars into a tripod, allowing motion in three orthogonal directions. To achieve tunneling, the sample is moved toward the tip at 0.15 μm per step by means of a stepper motor through a gear reduction mechanism. This UHV STM operates in the constant current mode.

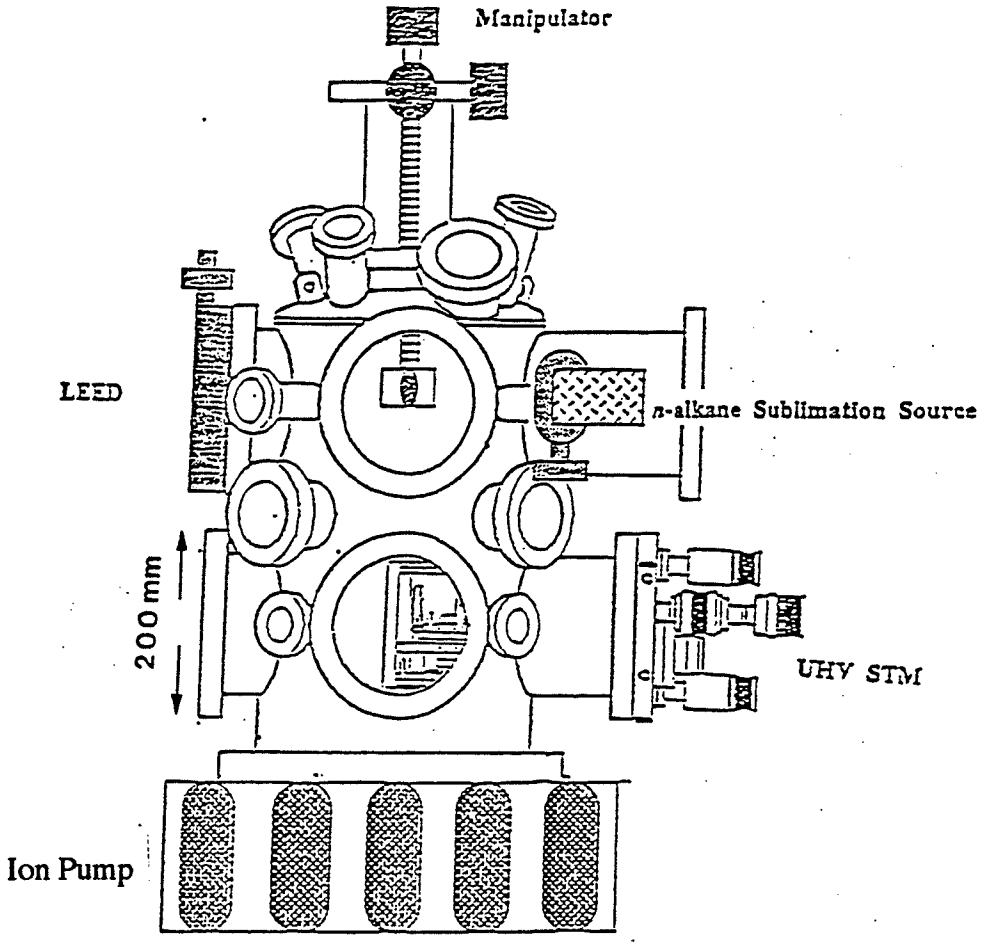

Figure 4.2 The complete UHV STM system. Bottom diagram show a detailed outline of the *n*-alkane sublimation port. Dimensions of the glass tube are $l = 25$ mm and $w = 15$ mm.

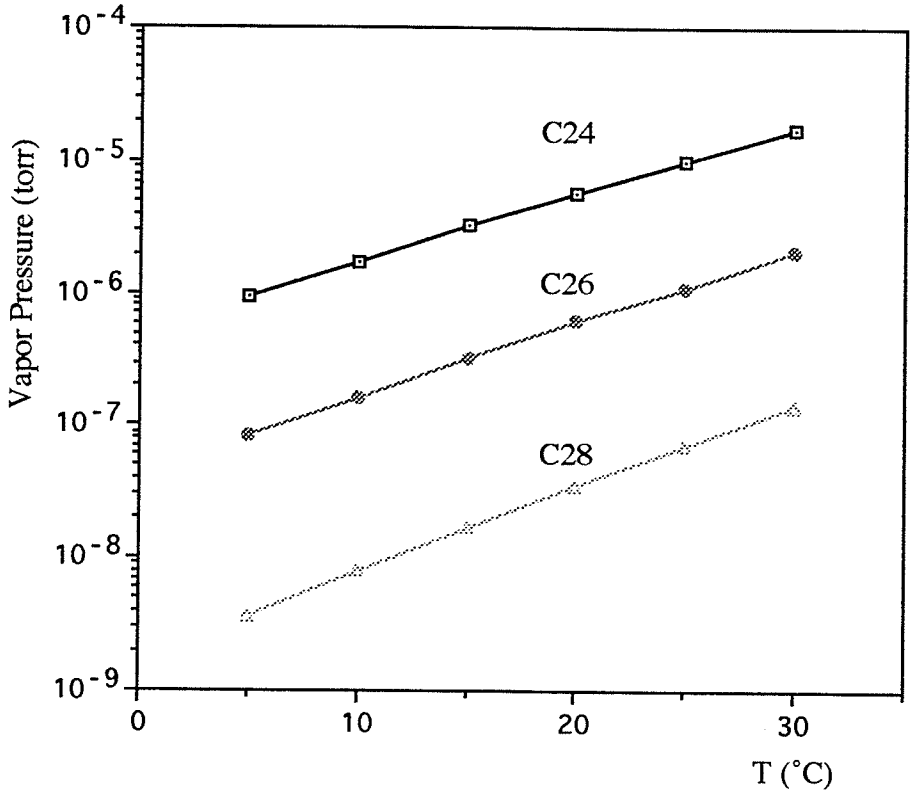

Figure 4.3 Vapor pressures of n-$C_{24}H_{50}$, n-$C_{26}H_{54}$ and n-$C_{28}H_{58}$ as a function of temperature.

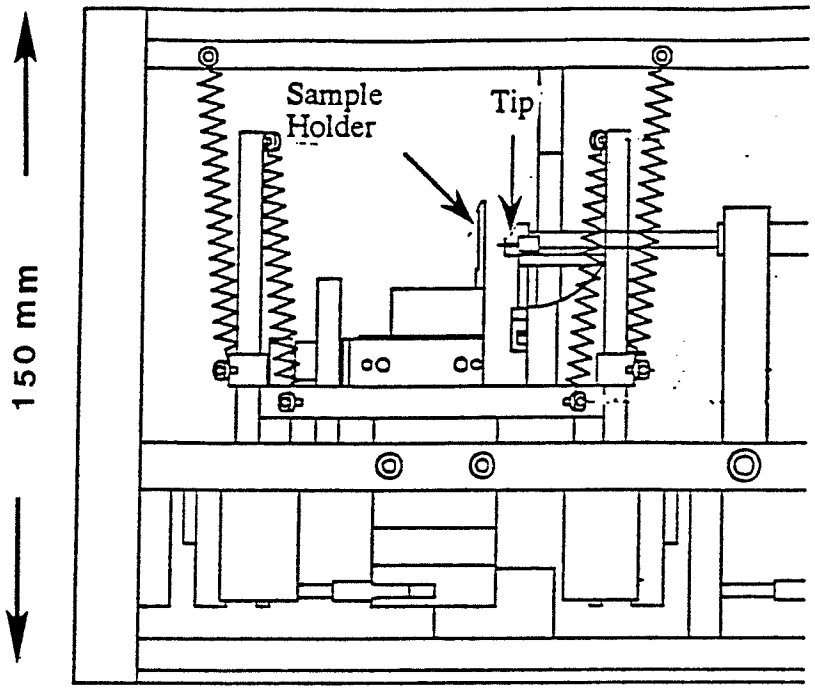

Side View of the Spring Suspension System

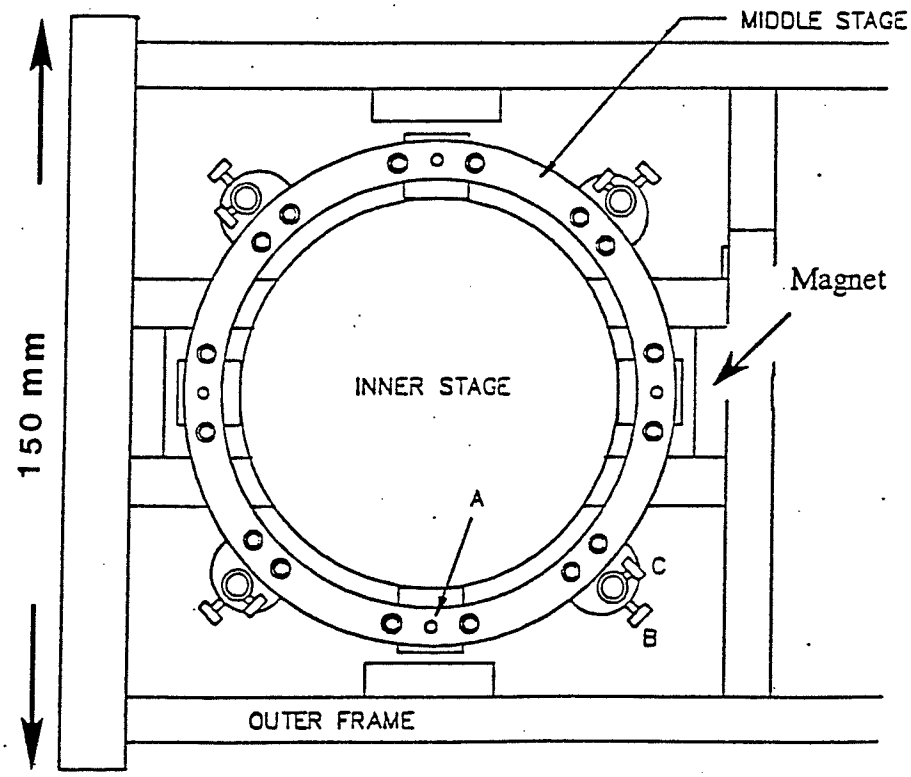

Figure 4.4 Park Scientific™ UHV STM-SU2

4.3 Sample Preparation

A thin sheet of graphite approximately 5 mm x 5 mm x 1 mm is mounted on a molybdenum holder and placed on the manipulator sample holder. The chamber is then pumped to a pressure of less than 1 x 10^{-9} torr. The graphite is heated to a temperature of 370 °C for 4 hours, with the chamber pressure maintained below 5 x 10^{-8} torr. LEED is performed on the graphite after the substrate is cleaned, showing the typical ring-like pattern at 74 eV incident electron beam; as shown in Figure 4.5. With the cleaned substrate mounted on the manipulator, *n*-$C_{26}H_{54}$ is then sublimated onto the graphite. The LEED was repeated every 0.5 hour to check if any changes can be observed in the LEED pattern. The time required to observe changes is approximately 3.5 hours, and the LEED showed a rather disordered pattern. This is used to give an indication that molecules are adsorbed on the surface. The sample is then loaded onto the UHV STM stage.

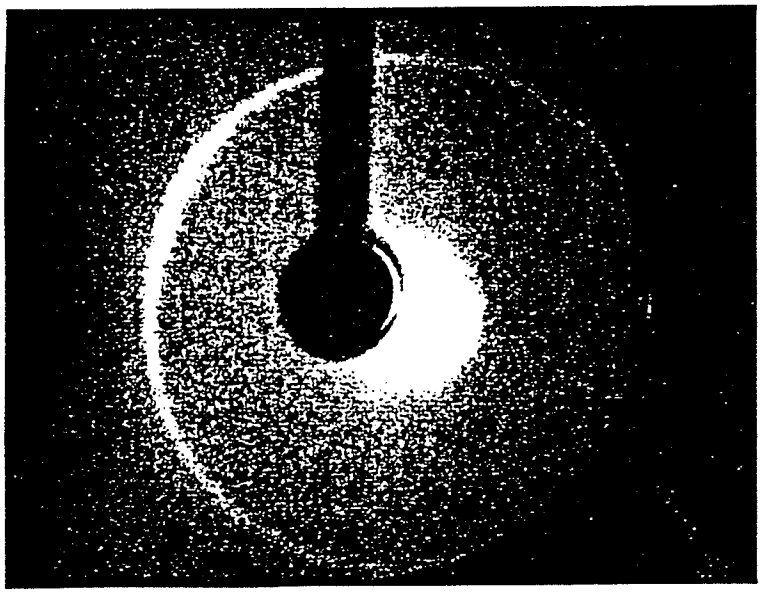

Figure 4.5 LEED of clean graphite. The poor quality of this figure is due to poor printing.

4.4 Result I

Figures 4.6(a) and (b) show 60 Å x 60 Å STM images obtained at a bias voltage of -0.65 V and 4.3 nA. Small clusters of unknown adsorbates are observed together with the graphite lattice. The dimensions of the largest cluster (see Figure 4.6(a)) are measured to be 40 Å long and 10 Å wide. The height of this cluster is about 15 Å. We are not able to determine the origin of these clusters at this time. In recent inverse photoemission spectroscopy studies of organic molecules adsorbed on solid surfaces, damage to the adsorbate systems due to the impact of incident low energy electron beam were observed [72, 73]. It is possible that this process occurred during the sample preparation stage of this experiment. The LEED experiment during the sublimation process might have caused the fragmentation of the *n*-$C_{26}H_{54}$ molecules on the graphite surface. These fragments of the molecules could then bonded to form these clusters. This possibility is addressed in a LEED-free experiment described in section 4.5.

An investigation of the surfaces of bulk (large crystals) of *n*-alkanes with STM has shown the formation of solid layers and crystalline-like structures from sample of various chain lengths [74]. We could also interpret our STM images as the crystalline structures of fragments of *n*-$C_{26}H_{54}$ molecules. Since the height of the cluster is approximately 15 Å, this would be then a 3-layer structure as the diameter of an *n*-alkane is 5 Å. These results are by no mean conclusive. In the next section however, a set of data from a different sample preparation technique is presented to show the evidence of ordered structure of *n*-alkanes adsorbed on graphite in UHV.

60 Å x 60 Å

Figure 4.6(a) UHV STM image of *n*-$C_{26}H_{54}$ on graphite, possibly showing a crystalline *n*-alkane phase.

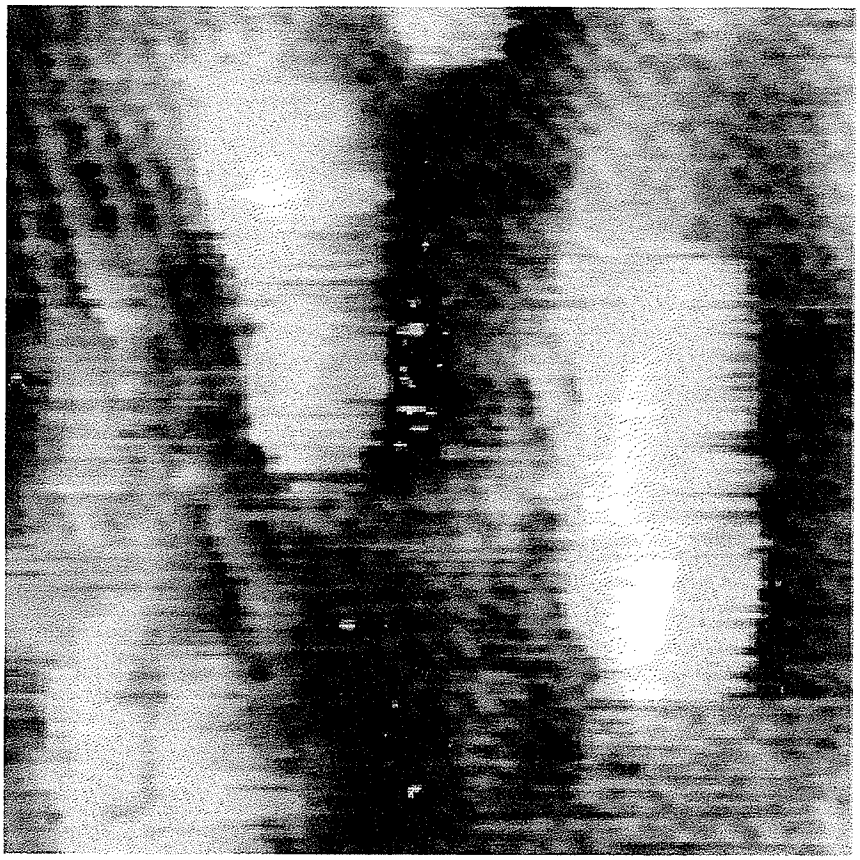

60 Å x 60 Å

Figure 4.6(b) UHV STM image of *n*-$C_{26}H_{54}$ on graphite, possibly showing a crystalline *n*-alkane phase.

4.5 Result II

To avoid performing LEED on the adsorbate covered graphite surface, the sublimation port is moved to a position where it is in the line of sight of the STM stage. The procedure for cleaning the substrate remained the same. After the cleaned graphite is loaded onto the STM stage, a STM experiment is carried out on the surface. Figure 4.7 shows a 900 Å x 900 Å image of the cleaned graphite surface. The image reveals some flat terraces on the surface. A contour plot across these terraces indicates that the step on each terrace is approximately 3 Å high. Thus we have observed the atomic steps on the graphite surface.

After the integrity of the substrate is verified with the STM, i.e. surface is free of defects, the gate valve is then opened to begin the sublimation of *n*-$C_{26}H_{54}$ molecules. STM experiments are done on the substrate surface at 0.5 hour intervals, with the gate valve opened. Only graphite lattice is observed for the first 3.5 hours. Figure 4.8 shows an image taken immediately after 4 hours of sublimation time. The bias voltage is -0.56 V and the tunneling current is 2.5 nA. This 320 Å x 320 Å image indicates that an ordered structure is formed on the surface. Some drift in the piezoelectric scanner is evident from this image as the ordered structure is curved at the lower part of the image. Notice that both left and right margins of the image are bright. This is due to the tip scanning across a large area of the surface during which the piezoelectric elements produce a parabolic type track with a minimum in the middle of the image. When the scan area is reduced to 160 Å x 160 Å, a better image of the ordered structure is obtained; as shown in Figure 4.9(a). This image is taken at -0.9 V and 3 nA shows a set of periodic bright bands. The width of these bands measured perpendicularly across the dark troughs is approximately 30 Å. This agrees well with the expected length of a *n*-

$C_{26}H_{54}$ molecule (32 Å). Attempts were made to improve the quality of the image by changing the bias voltage. As we can see in Figure 4.9(b), the attempts were unsuccessful. Although the images do not give striking features such as those *n*-alkane observed at the liquid/graphite interface, where each molecule is clearly resolved in the image, the present STM results do show that ordered structure of long chain *n*-alkanes can be observed on graphite surface at room temperature in an UHV environment. The lack of molecular resolution in the direction parallel to the dark troughs may be due to the surface mobility of the molecules as predicted. However, the presence of the troughs show that the molecules are relatively constrained to move in the direction parallel with their long axes. The preliminary data give evidence that molecules are lying parallel to the substrate and formed band-like structure similar to those observed at the liquid/graphite interface.

In order to improve the quality of the image in the future, the W tip is to be freed of contaminants. This can be done with technique such as the electron beam heating of the tip in vacuum. Also, a quartz-crystal microbalance is required to monitor the thickness of the adsorbed molecules during the sublimation process. If longer chain *n*-alkanes (more than 26 carbon atoms) are to be examined, a heating instrument is needed in order to raise the vapor pressure of these *n*-alkanes for successful sublimation of the molecules onto surfaces. We have just shown that UHV STM imaging of long chain *n*-alkanes on graphite at room temperature is possible. This work can be extended to imaging *n*-alkanes on Ag and Au metal surfaces. Previous LEED studies showed that *n*-C_4H_{10} and *n*-C_8H_{18} molecules formed an ordered monolayer on Ag(111) in the temperature range 100 - 200 K [75]. The long chain *n*-alkanes could be stable when adsorbed on Au and Ag surfaces at room temperature. The movement of the *n*-$C_{40}H_{82}$ molecule is estimated to be 1×10^{-3} Å/s at room temperature on a Ru surface [76]. This

makes the long chain *n*-alkanes adsorbed on Au and Ag an ideal system for STM study.

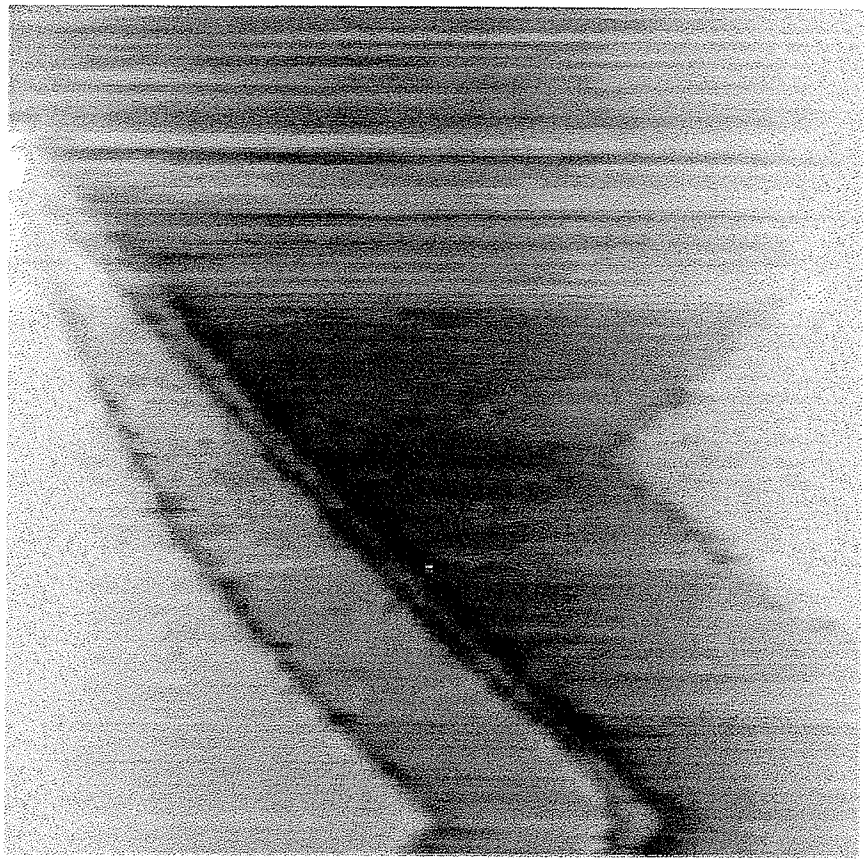

900 Å x 900 Å

Figure 4.7 Image of graphite showing the atomic steps.

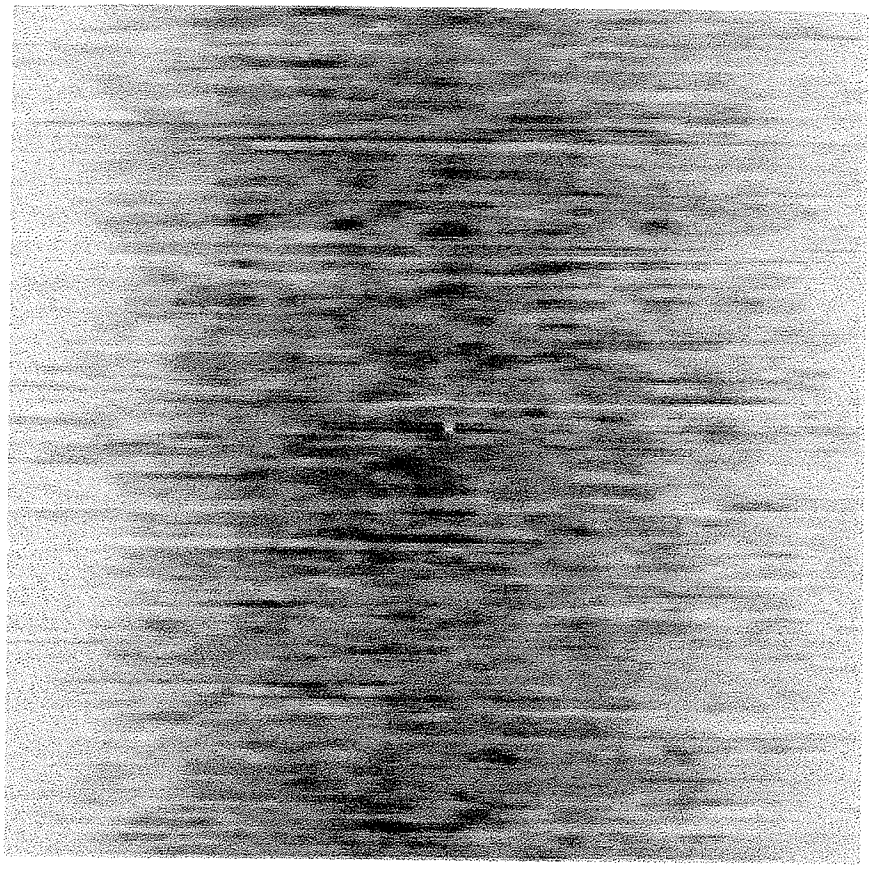

320 Å x 320 Å

Figure 4.8 STM image of n-$C_{26}H_{54}$. Ordered structure is visible in this image.

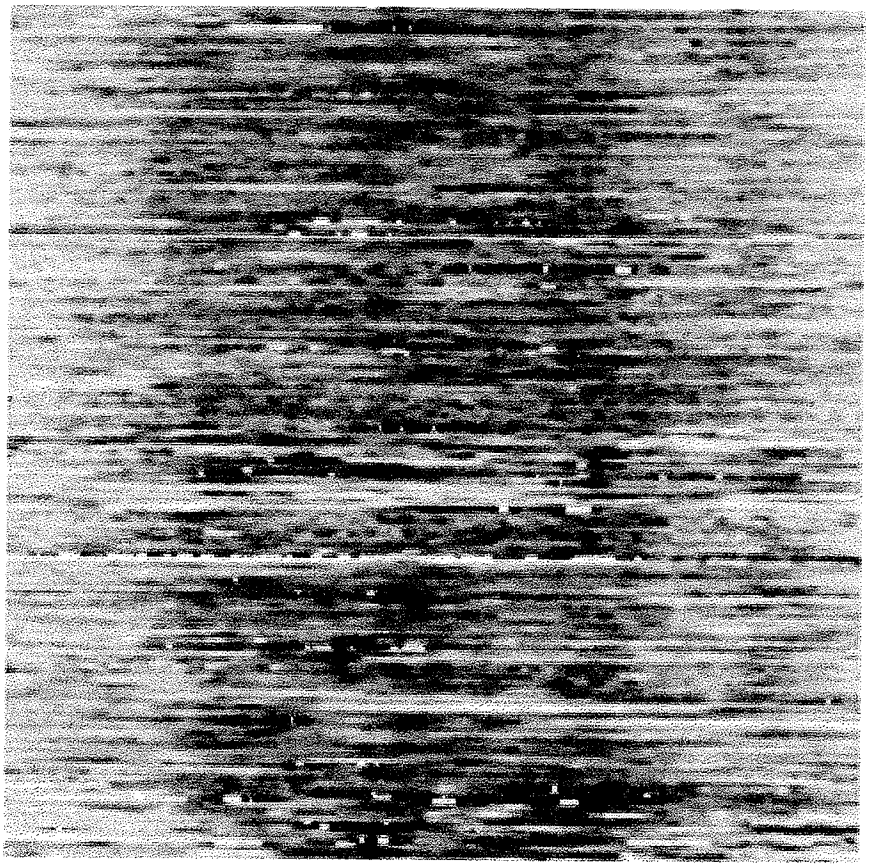

160 Å x 160 Å

Figure 4.9(a) Structure of adsorbed *n*-$C_{26}H_{54}$ showing band-like feature.

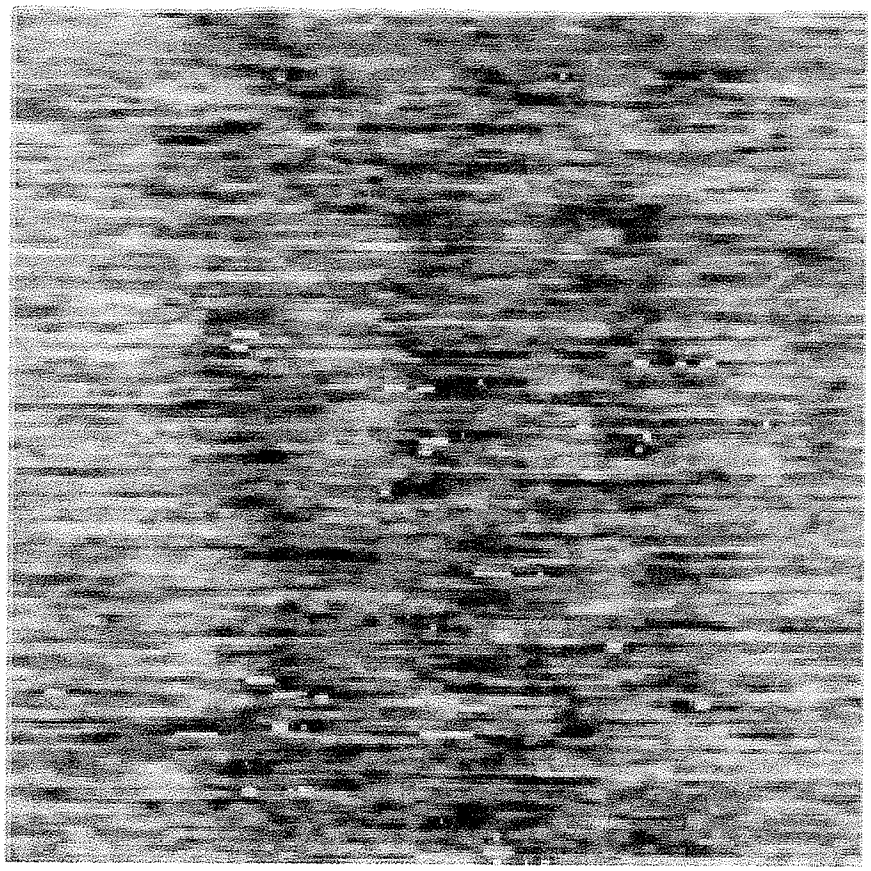

160 Å x 160 Å

Figure 4.9(b) Image at different voltage, but cannot resolve individual molecule.

Chapter 5 Imaging Mechanism

What gives rise to the image contrast observed in the STM imaging of molecules? This is a challenging and yet an unanswered question. As described in Chapter 1, numerous imaging mechanisms have been proposed for imaging molecules. These include resonant tunneling [13], local modification of the substrate LDOS due to the presence of the adsorbed molecules [8], and the contribution of atomic and molecular orbitals to the total tunneling conductance [10, 11]. It might very well be that the imaging mechanism depends on the particular system under study. For example, it is likely that molecules physisorbed on surfaces will yield different imaging mechanism than those of the chemisorbed systems; and the size of the adsorbates could also be a crucial factor.

It is difficult to present an all encompassing theory to explain all the STM images of molecules observed in this thesis work. It is not impossible however, to demonstrate using one of the models above and to give some insights into the imaging mechanism. The resonant tunneling model [13] is chosen and presented below.

This resonant tunneling model was first proposed by W. Mizutani. It assumes that the tunneling current is modulated by the molecular orbitals of the adsorbed molecules. This model was used to explain the imaging of liquid crystals on a graphite surface. We have chosen to model the *n*-decanols physisorbed on graphite system in the same way as the liquid crystal/graphite system by W. Mizutani. The tip and substrate are modeled as a free electron gas and the molecule is modeled as a square well potential. The dimensions of this model are shown in Figure 5.1, where d_{m} is the diameter of the molecule, d_{tm} and d_{ms} are the tip-molecule and molecule-substrate separations respectively. To represent this system, consider the one-dimensional square well as shown in Figure 5.2(a). In this case the left and right electrodes represent the tip and

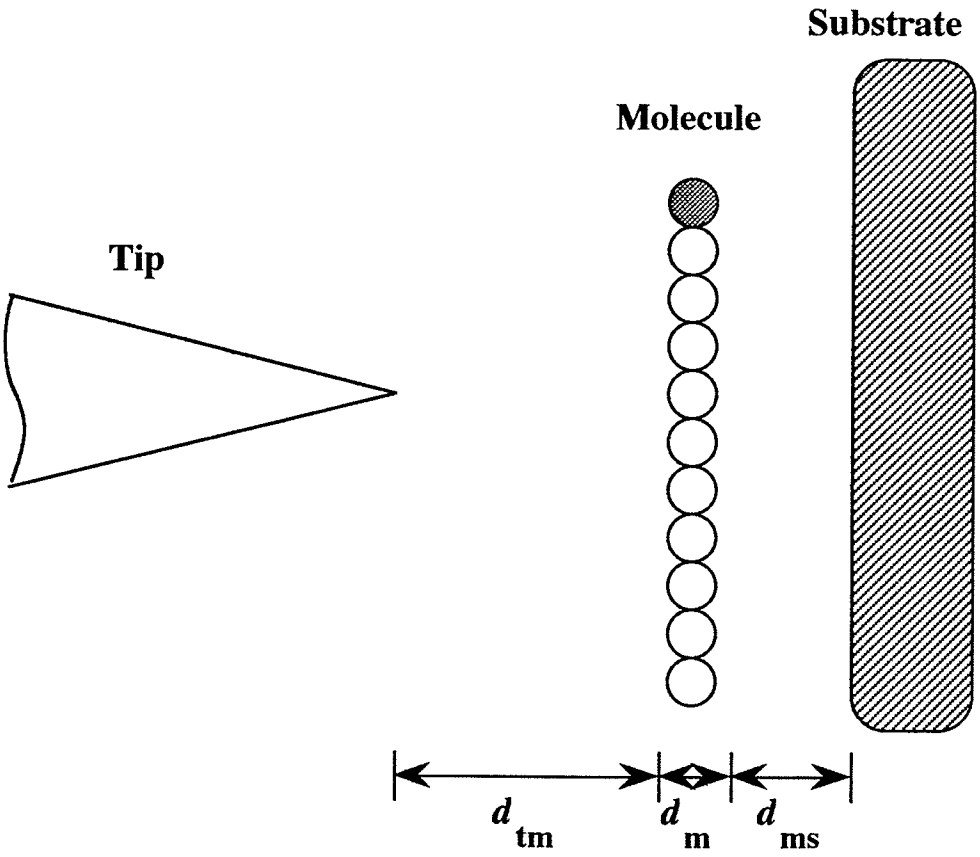

Figure 5.1 Physical system under consideration. The open circles are the carbon atoms while the shaded circle represents the OH head group of the *n*-decanol molecule.

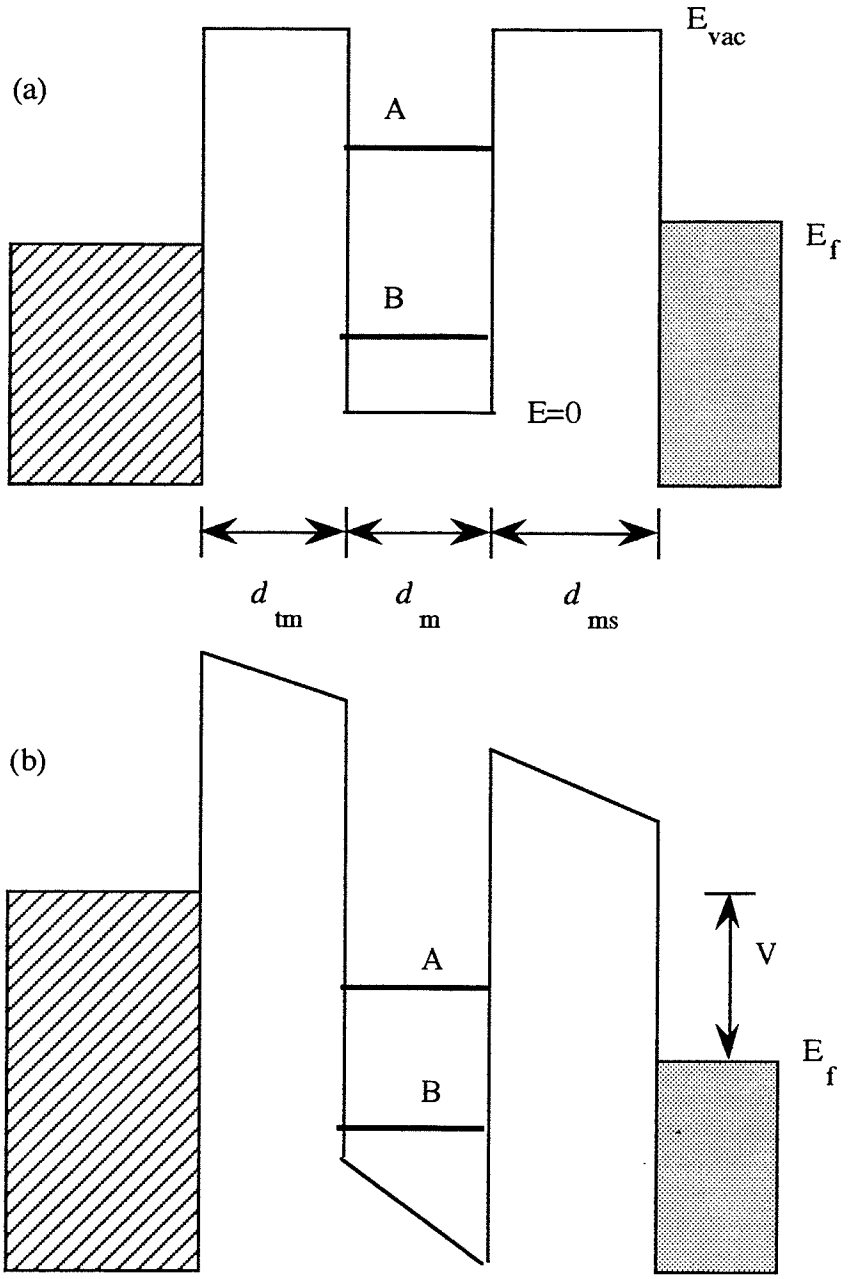

Figure 5.2 Resonant tunneling model representing the physical system.

A and B represent two energy levels inside the potential well.

graphite substrate respectively. Assume that there exists an energy level A which corresponds to one of the molecular orbitals in the potential well. When a bias is applied to one of the electrodes, electrons can tunnel from one electrode to another. If the applied voltage is such that the tunneling electron has an energy equal to the energy level of the molecule, the transmission through the barrier can be increased by orders of magnitude, as in the case of Figure 5.2(b). This large enhancement in the transmission probability is called the resonant tunneling phenomena. However even well below this voltage, there is a measurable effect on the tunneling current. From the WKB and transfer matrix method, it has been shown that at zero temperature and neglecting the effect of image force on the rectangular potential barrier, the transmission probability is given by [13]

$$T(E)^{-1} = \cosh^2 x_1 \cosh^2 x_3 + \sinh^2 x_1 \sinh^2 x_3 + 2 \cosh x_1 \cosh x_3 \sinh x_1 \sinh x_3 \cos x_2$$

where $$x_1 = \frac{1}{\hbar}\sqrt{2m\,(E_{vac}-E)}\; d_{tm}$$

$$x_2 = \frac{2}{\hbar}\sqrt{2m\,E}\; d_{m}$$

$$x_3 = \frac{1}{\hbar}\sqrt{2m\,(E_{vac}-E)}\; d_{ms}$$

and the current density is

$$J(V) = \frac{me}{2\pi^2\hbar^3}\left[eV\int_{-eV}^{E_f-eV} T(E+eV)\,dE + \int_{E_f-eV}^{E_f}(E_f - E)\,T(E+eV)\,dE\right]$$

m = electron mass, E = electron energy, with $E = 0$ being the bottom of the square well potential, E_{vac} = vacuum level, E_f = Fermi level, e = electron charge, h = Planck constant and V = bias voltage.

Consider the left electrode to be the W tip, and the *n*-decanol (*n*-$C_{10}H_{21}OH$) molecules physisorbed on the graphite surface. We can use what is known about the system of *n*-alkanols adsorbed on solid surfaces to help choose the parameters which we will use for the simulation. The tip-molecule separation d_{tm} and the molecule-substrate separation d_{ms} are chosen to be 5 Å and 4 Å respectively [10]. From inverse photoemission spectroscopy studies, the lowest unoccupied molecular orbital (LUMO) of the *n*-alkane portion of the molecule (*n*-alkane tail) is located just above the E_{vac}, and the highest occupied molecular orbital (HOMO) is approximately 10 eV below the LUMO [15]. If we choose d_m = 2.8 Å, we can obtain two energy levels separated by 10 eV. The width d_m is adjusted to 2.8 Å to generate two energy levels 10 eV apart inside the well to simulate tunneling through the *n*-alkane. As shown in Figure 5.3, *T(E)* with d_m = 2.8 Å gives two transmission peaks separated by an amount of 10 eV, and we model these peaks as the LUMO and HOMO of the *n*-alkane tails. E_{vac} is therefore located at 11 eV. Since the work function of graphite has been measured to be around 5 eV [77], then $E = 6$ eV corresponds to the Fermi level (E_f) of the graphite in our model. Electron impact energy loss spectra of *n*-alkanols shows a 3s OH anti-bonding state lying close to 3 eV below E_{vac} [78]. We can lower the energy of the LUMO in our model molecule by 3 eV using d_m = 3.2 Å. With d_m = 3.2 Å, a peak about 3 eV below the E_{vac} is generated which we will use as the 3s OH anti-bonding state; as shown superimposed in Figure 5.3. It is important to note that the characteristic of the *T(E)* curve does not change with d_{tm}. Figure 5.4 displays *T(E)* for several d_{tm}, and it

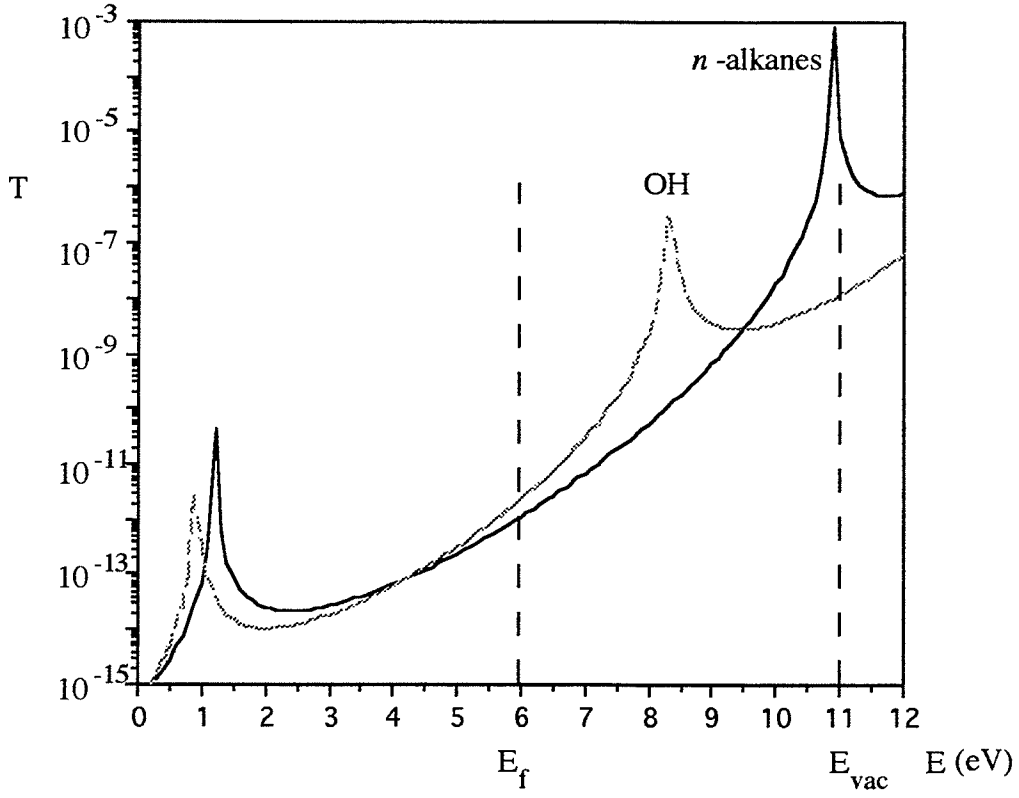

Figure 5.3 Transmission probability calculated from the resonant tunneling model. d_m = 2.8 Å gives two energy levels separated by 10 eV to represent the LUMO and HOMO of the *n*-alkane. d_m = 3.2 Å gives an energy level close to 3 eV below the E_{vac}. The Fermi level of graphite is located at 6 eV.

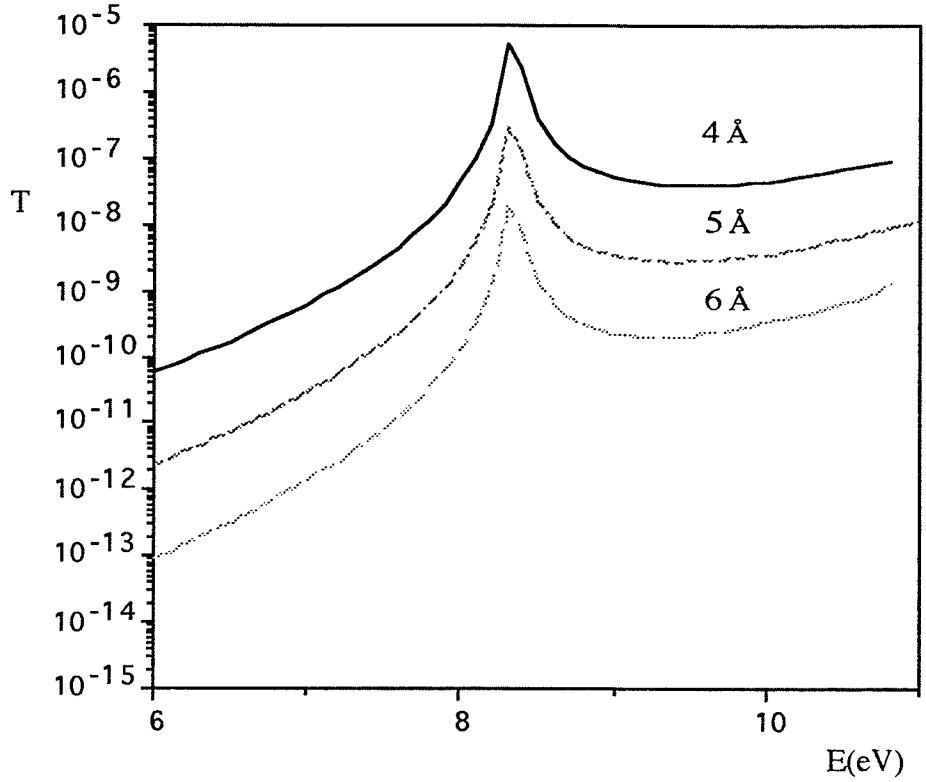

Figure 5.4 Transmission probability for three different tip-molecule distances d_{tm}.

shows that the transmission peak (energy level) changes in magnitude but remains fixed in energy. The current density $J(V)$ is then calculated from $V = 0$ to $V = 2$ V for d_m = 2.8 Å and 3.2 Å. The results are shown in Figure 5.5. In absence of the molecule, i.e. if we let $d_m = 0$, $J(V)$ is plotted in Figure 5.5 (c). All the current densities display a similar characteristics from 0 to 2 V. A noticeable difference in the magnitude of the current density between tunneling through the *n*-alkane and the OH can be seen in this figure. Note that the magnitude of $J(V)$ from the calculation is small compared with the experimental value. These can be made comparable by decreasing d_{tm} and not altering the characteristic of the tunneling current.

The presence of the molecules obviously has an effect on the tunneling current. We will now estimate this effect on an STM image. To do this, we need to calculate the change in separation in the tunnel junction. As mentioned earlier, the dependence of the tunneling current on separation is generally the following form

$$I \propto V \exp(-A\phi^{1/2}s)$$

where A=1.025 $(\text{eV}^{1/2}\text{Å})^{-1}$ and ϕ is the average work function of the electrodes. Taking ϕ_w = 4.55 eV [79] and $\phi_{graphite}$ = 5 eV, the calculated change in the tunnel junction separation Δs is shown in Figure 5.6. When imaging in the constant current mode, any increase in the tunneling current will result in the tip moving away from the the substrate in order to maintain constant current, thus yielding contrast in the STM image. Figure 5.6 shows that Δs is significantly larger when a molecule is present in between the tunnel junction; even before resonant tunneling occurs. As the tip scans over the surface where a molecule is present, the tip will retract due to the increase in tunneling current. This increase in the tunneling current causes large Δs and therefore giving

higher contrast in the STM image that reflects the adsorbed molecules. Although the 3s OH state is situated far away (>2 eV) from the Fermi level of graphite, the calculation shows that the effect of this state on Δs can be observed below its energy. Similarly for the *n*-alkane tails, which is further away from the Fermi level; a significant change in Δs can also be seen from 1 to 2 V. Note that the Δs due to the 3s OH state is larger than that of the *n*-alkane tails. This shows that the OH head groups should be easier to observe than the *n*-alkane tails, which agrees with our experimental results. Figure 5.7 gives an pictorial illustration of the calculated results. At low voltages (<1 V), the separation between the tip and the substrate surface is essentially unchanged regardless of the presence of the molecule. At higher voltages, when the tip is on top of the *n*-alkane portion of the molecule, an increased in the tunneling current causes the tip to retract in order to maintain constant tunneling current. Similarly when the tip is on top of the OH head group, a strong enhancement in the current causes large Δs. From our calculations, the Δs due to the OH group is larger than that of the *n*-alkane tail. Therefore the OH head group will appears brighter (higher contrast) than the *n*-alkane tail and the graphite lattice in the STM image. These calculations however do not quite explain why we can observe the *n*-decanol molecules at low voltages (< 0.5 V). Recent calculations based on the local density approximation gave evidence that the molecular orbitals of atoms or molecules adsorbed on surfaces shift and spread in energy such that they are within the tunneling range [11]. It was shown that in the case of imaging Xe atoms on Ni(110) surface, although the 6s Xe resonance is located near the vacuum level (4 eV above the Fermi level of Ni), calculations showed that the broadening of this resonance resulted in additional Xe 6s states near the Fermi level. Therefore the Xe atoms can be imaged with the STM at small voltages. It is possible that the broadening of the 3s OH and the LUMO of the *n*-alkanes occurs such that these states lie closer to the Fermi level of graphite and

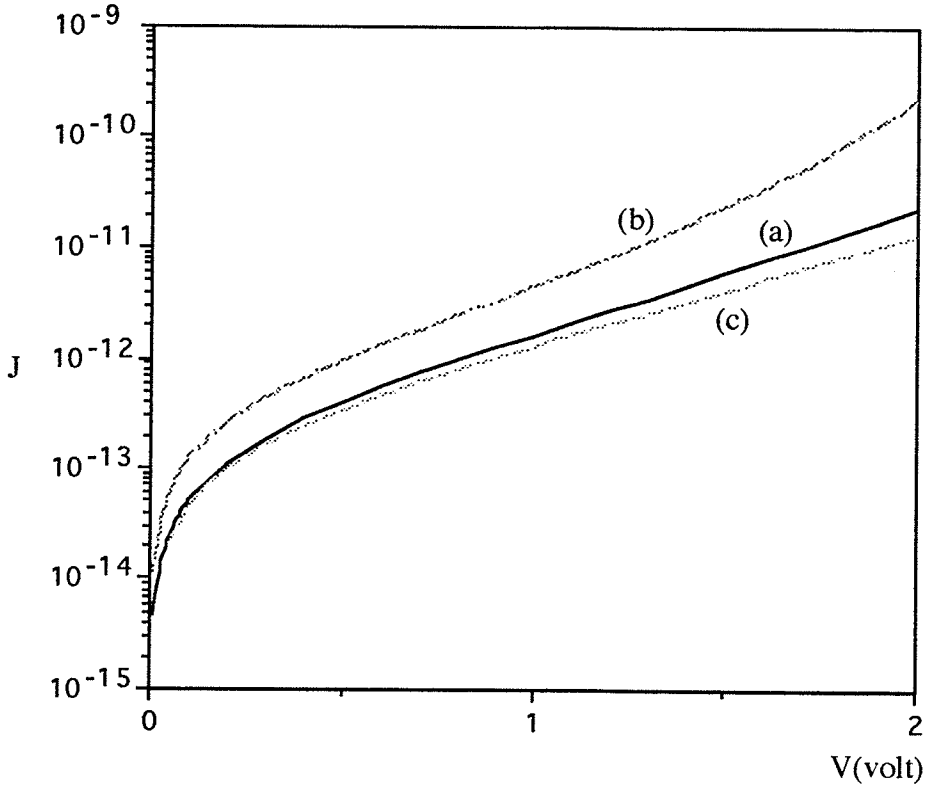

Figure 5.5 Current density as a function of voltage for tunneling through the (a) *n*-alkane, (b) OH and (c) without the molecule. Unit of J is A/nm^2.

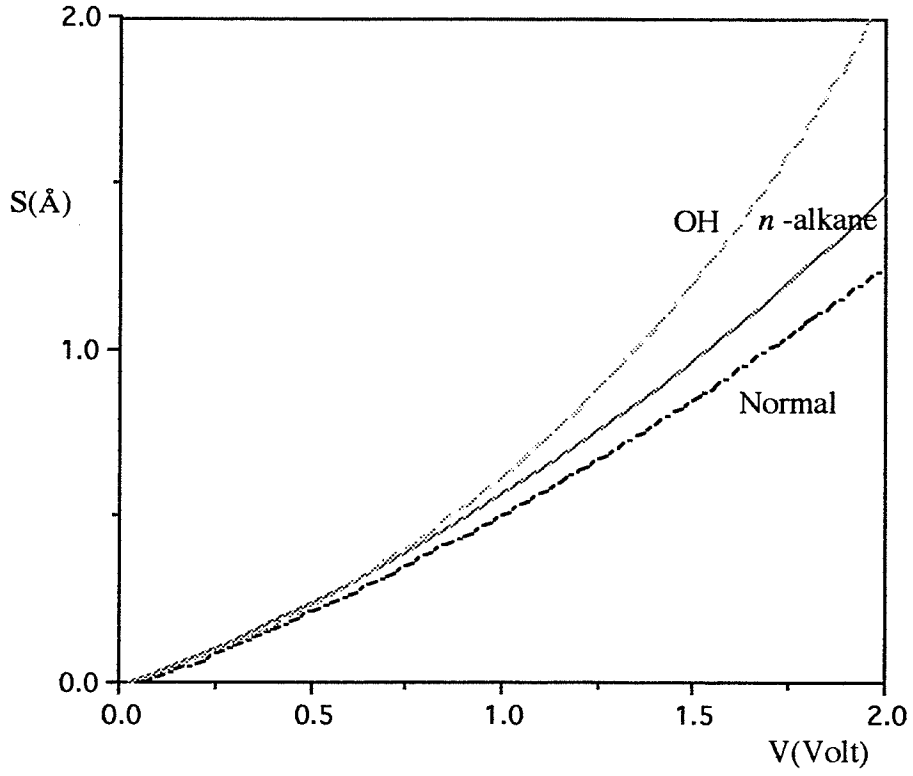

Figure 5.6 Change in height as a function of voltage. The *Normal* curve is from $d_m = 0$.

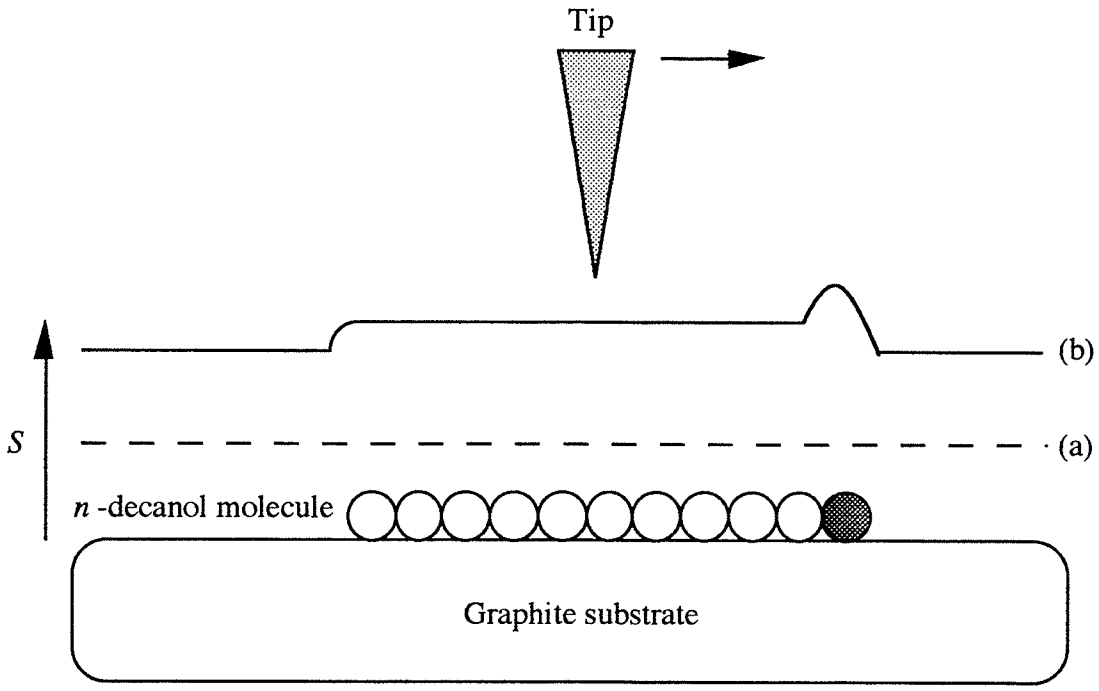

Figure 5.7 Schematic illustration of the change in the position of the tip when scans from left to right. Open circles are the carbon atoms of the *n*-alkane tail and shaded circle is the OH head group. (a) At low voltages, *s* remains unchanged. (b) At higher voltages, *s* changes due to the increase in the tunneling current when the tip in on top of the molecule.

thus can be imaged with the STM. It is still not well understood how differing electronic structures associated with different functional groups of a molecule would be reflected in a STM image. As we have shown in the case of imaging *n*-decanol, intramolecular imaging of chemically inequivalent functional groups within a molecule is possible. The question of "Why molecules are bright" is not an easy one, let alone "Why half of a molecule is bright".

Finally, some remarks on the imaging mechanism of self-assembled molecules. Since the molecules are adsorbed perpendicularly to the substrate, the spacing between the tip and the substrate is now drastically increased. We have successfully imaged *n*-decanol (length ~ 14Å) and *n*-dodecanol (length ~ 17 Å) on Au(111) surfaces. Longer chain length molecules such as the $C_{18}H_{37}SH$ (length ~ 25 Å) can be imaged with the STM [51]. The tunneling process between a molecule lying parallel or perpendicular to the substrate could be different. In the first case, 'through space' tunneling is responsible due to the spatial overlapping of the tip-molecule-substrate wavefunctions. The latter case however, a 'through bond' tunneling process is likely possible, i.e. tunneling arises from the electron transfer within the molecule. Based on the Elastic Scattering Quantum Chemistry (ESQC) calculation, it was shown that through bond tunneling gives rise to resonant peaks in the transmission probability [80]. These resonant peaks correspond to the molecular orbitals of the molecules situated perpendicularly between two electrodes. As mentioned earlier, the imaging mechanism could depend on the size of the the adsorbates. Perhaps each system under studied yields its own unique interpretation of the imaging mechanism.

Conclusions

As we have shown in this work, the STM can provide detailed structural information of simple organic molecules adsorbed at the liquid/solid interface. Initial results from STM imaging of *n*-alkanes in UHV give indication that the structural ordering of the molecules is similar to those previously observed at the liquid/graphite interface.

The imaging mechanism associated with the STM imaging of molecules remains unresolved. Although a simple resonant tunneling calculation can explain some of the experimental results, it is however inadequate. The role of chemically inequivalent functional groups within a molecule giving rise to different contrast is still unclear. We have shown that functional groups can be independently imaged at different voltages. To give *the* ultimate illustration, Figure C shows a 60 Å x 60 Å image of *n*-decanol at the liquid/graphite interface. At 0.58 V and 0.26 nA, the image contrast yields the position of the OH functional groups. Each dark hole corresponds to one OH head group. It is clearly shown from this image that the OH groups are arranged in an alternate row fashion. Separation between two adjacent holes is approximately 5 Å, which agrees well with the diameter of the molecule. However, unlike previously shown (see Figure 3.5) in Chapter 3, this image reveals the graphite lattice but not the hydrocarbon tails of the adsorbed layer. The imaging parameters and conditions such as the bias voltage, tunneling current, temperature and the integrity of the tip can have influences on the outcome of an image. Under specific conditions, an image like Figure C can be obtained. Some say "a picture is worth thousand words", but Figure C represents in this case, countless equations and endless computation time.

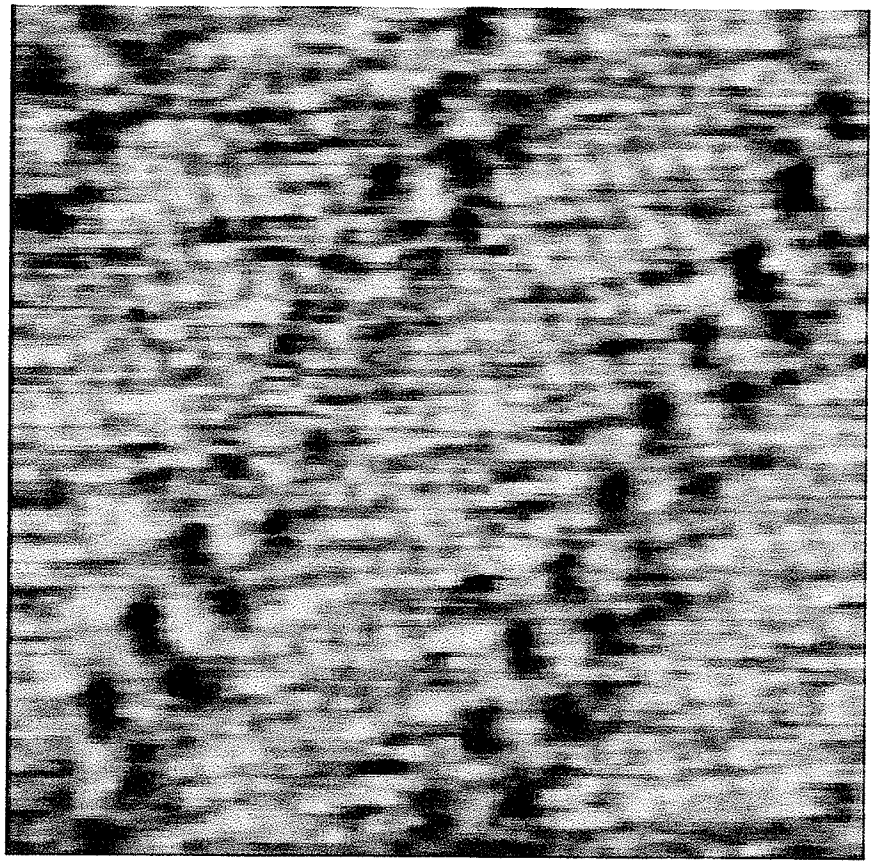

Figure C 60 Å x 60 Å STM image of *n*-decanol showing the OH head groups as dark holes.

References

[1] G. Binnig, H. Rohrer, Ch. Gerber and E. Weibel, *Phys. Rev. Lett.* 49 (1982) 57.

[2] G. Binnig and H. Rohrer, *Surf. Sci.* 126 (1983) 236.

[3] *Introduction to Scanning Tunneling Microscopy*, C. Julian Chen, *Oxford Univ. Press*, New York 1993.

[4] *Scanning Tunneling Microscopy*, J. A. Stroscio and W. J. Kaiser Ed., *Academic Press Inc.*, San Diego 1993.

[5] *Scanning Tunneling Microscopy I & II*, H. J. Güntherodt and R. W. Wiesendanger Ed., *Springer-Verlag*, Germany 1992.

[6] J. Tersoff and D. R. Hamann, *Phys. Rev.* B31 (1985) 805.

[7] J. Bardeen, *Phys. Rev. Lett.* 6 (1961) 57.

[8] J. K. Spong, H. A. Mizes, L. J. LaComb Jr., M. M. Dovek, J. E. Frommer and J. S. Foster, *Nature* 338 (1989) 137.

[9] D. P. E. Smith, J. K. H. Hörber, G. Binnig and H. Nejoh, *Nature* 344 (1990) 641.

[10] A. J. Fisher and P. E. Blöchl, *Phys. Rev. Lett.* 70 (1993) 3263.

[11] D. M. Eigler, P. S. Weiss, E. K. Schweizer and N. D. Lang, *Phys. Rev. Lett.* 66 (1991) 1189.

[12] S. M. Lindsay, O. F. Sankey, Y. Li and C. Herbst, *J. Phys. Chem.* 94 (1990) 4655.

[13] W. Mizutani, M. Shigeno, M. Ono and K. Kajimura, *Appl. Phys. Lett.* 56 (1990) 1974.

[14] G. C. McGonigal, R. H. Bernhardt and D. J. Thomson, *Appl. Phys. Lett.* 57 (1990)

[15] R. Dudde and B. Reihl, *Chem. Phys. Lett.* 196 (1992) 91.

[16] P. S. Weiss and D. M. Eigler, *Phys. Rev. Lett.* 69 (1992) 2240.

[17] J. A. Stroscio, R. M. Feenstra and A. P. Fein, *Phys. Rev. Lett.* 58 (1987) 1668.

[18] L. J. Whitman, J. A. Stroscio, R. A. Dragoset and R. J. Celtotta, *Phys. Rev. Lett.* 66 (1991) 1338.

[19] D. F. Ogletree, C. Ocal, B. Marchon, G. A. Somorjai, M. Salmeron and W. Siekhaus, *J. Vac. Sci. Technol.* A8 (1990) 297.

[20] S. L. Yan, X. Gao, S. C. Chang, B. C. Schardt and M. J. Weaver, *J. Am. Chem. Soc.* 113 (1991) 6049.

[21] C. M. Vitus, S. C. Chang, B. C. Schardt and M. J. Weaver, *J. Phys. Chem.* 95 (1991) 7559.

[22] V. M. Hallmark, S. Chiang, J. K. Brown and C. Woll, *Phys. Rev. Lett.* 66 (1991) 48.

[23] V. M. Hallmark, S. Chiang and C. Woll, *J. Vac. Sci. Technol.* B9 (1991) 1111.

[24] D. P. E. Smith, J. K. H. Hörber, G. Binnig and H. Nejoh, *Narture* 344 (1990) 641.

[25] J. S. Foster, J. E. Frommer and P. C. Arnett, *Nature* 331 (1988) 324.

[26] H. Sotobayashi, T. Schilling and B. Tesche, *Langmuir* 6 (1990) 1246.

[27] D. P. E. Smith, A. Bryant, C. F. Quate, J. P. Rabe, C. Gerber and J. D. Swalen, *Proc. Natl. Acad. Sci. USA* 84 (1987) 969.

[28] C. A. Lang, J. K. H. Hörber, T. W. Hansch, W. M. Heckl and H. Mohwald, *J. Vac. Sci. Technol.* A6 (1988) 368.

[29] R. Yang, K. Naoi, D. F. Evans, W. H. Smyrl and W. A. Hendrickson, *Langmuir* 7 (1991) 556.

[30] B. A. Watson, M. A. Barteau, L. Haggerty, A. M. Lenhoff and R. S. Weber,

Langmuir 8 (1992) 1145.

[31] X. L. Wu and C. M. Lieber, *J. Phys. Chem.* 92 (1988) 5556.

[32] J. Mou, W. Sun, J. Yan, W. S. Yang, C. Liu, Z. Zhai, Q. Xu and Y. Xie, *J. Vac. Sci. Technol.* B9 (1991) 1566.

[33] M. J. Miler, T. McMaster, H. J. Carr, A. S. Tatham, P. R. Shwwry, J. M. Field, P. S. Belton, D. Jeenes, B. Hanley, M. Whittam, P. Cairns, V. J. Morris and N. Lambert, *J. Vac. Sci. Technol.* A8 (1990) 698.

[34] T. P. J. Beebe, T. E. Wilson, D. F. Ogletree, J. E. Katz, R. Balhorn, M. B. Salmeron and W. J. Siekhaus, *Science* 243 (1989) 370.

[35] R. W. Keller, D. D. Dunlap, C. Bustamante, D. J. Keller, R. G. Garcia, C. Gray and M. F. Maestre, *J. Vac. Sci. Technol.* A8 (1990) 706.

[36] T. Thundat, L. A. Nagahara, P. Oden and S. M. Lindsay, *J. Vac. Sci. Technol.* A8 (1990) 645.

[37] R. H. Bernhardt, *M. Sc. Thesis,* University of Manitoba (1990).

[38] S. Buchholz, H. Fuchs and J. P. Rabe, *J. Vac. Sci. Technol.* B9 (1991) 857.

[39] C. E. Brown, D. H. Everett, A. V. Powell and P. E. Thorne, *Faraday Discuss. Chem. Soc.* 59 (1975) 97.

[40] G. H. Findenegg, *J. Chem. Soc. Faraday Trans.* 68 (1972) 1799.

[41] S. Abrahamsson, G. Larsson and E. von Sydow, *Acta Crystallogr.* 13 (1960) 770.

[42] D. P. E. Smith, *J. Vac. Sci. Technol.* B9 (1991) 1119.

[43] J-C. Poulin and H. B. Kagan, *C. R. Acad. Sci. Paris* 313 (1991) 1533.

[44] K. Tanaka, T. Seto, A. Watanabe and T. Hayashida, *Bull. Inst. Chem. Res. Kyoto Univ.* 37 (1959) 281.

[45] T. Yamamoto, K. Nozaki and T. Hara, *J. Chem. Phys.* 92 (1990) 631.

[46] S. W. Barton, B. N. Thomas, E. B. Flom, S. A. Rice, B. Lin, J. B. Peng, J. B.

Ketterson and P. Dutta, *J. Chem. Phys.* 89 (1988) 2257.

[47] K. W. Herwig and F. R. Trouw, *Phys. Rev. Lett.* 69 (1992) 89.

[48] *An Introduction to Ultrathin Organic Films*, A. Ulman, *Academic Press Inc.*, New York 1991.

[49] G. M. Whitesides, *Abstract to AVS 39th National Symposium,* Chicago 1992.

[50] C. D. Bain, E. B. Troughton, Y. T. Tao, J. Evall, G. M. Whitesides and R. G. Nuzzo, *J. Am. Chem. Soc.* 111 (1989) 321.

[51] C. A. Widrig, C. A. Alves and M. D. Porter, *J. Am. Chem. Soc.*113 (1991) 2805.

[52] J. V. Sanders and D. Tabor, *Proc. R. Soc. London* 204 (1951) 525.

[53] C. D. Bain, J. Evall and G. M. Whitesides, *J. Am. Chem. Soc.* 111 (1989) 7155.

[54] In Figure 11.1, there is a slight angular distortion arising from our scanning piezoelectric elements.

[55] V. M. Hallmark, S. Chiang, J. F. Rabolt, J. D. Swalen and R. J. Wilson, *Phys. Rev. Lett.* 59 (1987) 2879.

[56]Q. Dai and J. Gellman, *Sur. Sci.* 257 (1991) 103.

[57] L. Strong and G. M. Whitesides, *Langmuir* 4 (1988) 546.

[58] C. E. D. Chidsey, G-Y. Liu, P. Rowntree and G. Scoles, *J. Chem. Phys.* 91 (1989) 4421.

[59] N. Camillone, C. E. D. Chidsey, G-Y, Liu and G. Scoles, *J. Chem. Phys.* 98 (1993) 3503.

[60] R. L. McCarley, Y-T., Kim and A. J. Bard, *J. Phys. Chem.* 97 (1993) 211.

[61] Y-T., Kim and A. J. Bard, *Langmuir* 8 (1992) 1096.

[62] Y. T. Tao, *J. Am. Chem. Soc.* 115 (1993) 4350.

[63] N. E. Schlotter, M. D. Porter, T. B. Bright and D. L. Allara, *Chem. Phys. Lett.* 132 (1986) 93.

[64] H. Ohtani, R. J. Wilson, S. Chiang and C. M. Mate, *Phys. Rev. Lett.* 60 (1988) 2398.

[65] R. J. Driscoll, M. G. Youngquist and J. D. Baldeshwieler, *Nature,* 346 (1990) 294.

[66] J. P. Rabe and S. Buchholz, *Science* 253 (1991) 424.

[67] J-P. Bucher, H. Roeder and K. Kern, *Surf. Sci.* 289 (1993) 370.

[68] J. Krim, J. Suzanne, H. Shechter, R. Wang and H. Taub, *Surf. Sci.* 162 (1985) 446.

[69] *Physics at Surfaces,* A. Zangwill, *Cambridge Univ. Press,* Great Britain 1988.

[70] F. Y. Hansen and H. Taub, *Phys. Rev. B* 19 (1979) 6542.

[71] A. V. Kiselev, *Discuss. Faraday Soc.* 40 (1965) 205.

[72] K. H. Frank, P. Yannoulis, R. Dudde and E. E. Koch, *J. Chem. Phys.* 89 (1988) 7569.

[73] R. Dudde, B. Reihl and A. Otto, *J. Chem. Phys.* 92 (1990) 3930.

[74] B. Michel, G. Travaglini, H. Rohrer, C. Joachim and M. Amrein, *Z. Phys.* B 76 (1989) 99.

[75] L. E. Firment and G. A. Somorjai, *J. Chem. Phys.* 69 (1978) 3940.

[76] J. L. Brand, M. V. Arena, A. A. Deckert and S. M. George, *J. Chem. Phys.* 92 (1990) 5136.

[77] B. Robrieux, R. Faure and J. P. Dussaulay, *C. R. Acad. Sci. Ser. B* 278 (1974) 659.

[78] W. C. Tam and C. E. Brion, *J. Electron. Spectrosc. Rel. Phen.* 3 (1974) 263.

[79] *CRC Handbook of Chemistry and Physics,* 68th Edition, R. C. Weast Ed. *CRC Press,* USA 1987 - 1988.

[80] C. Joachim and P. Santel, *Scanning Tunneling Microscopy and Related Methods,* R. J. Behm et al. (eds), *Kluwer Academic Publishers* 1990.

Appendix A

Imaging *n*-Decanol at the Oil/Graphite Interface

In the initial period of STM imaging of *n*-alkanes and *n*-alkanols at the liquid/graphite interface, it had been suggested that it is 'easier' to observe the ordered structures if imaged in a heavy fluid environment [A1]. The following are the results we obtained from imaging *n*-decanol in the presence of fluorinated pump oil (FPO). Sample preparation is done by first applied a few drops of pure *n*-decanol on the graphite surface. A drop of FPO is then added to the *n*-decanol/graphite interface. The assumption is that the adsorbed *n*-decanol monolayer is 'pinned' on the surface due to the presence of FPO.

Figure A1(a) and (b) show two typical images of *n*-decanol obtained under this environment. The scan size is 80 Å x 80 Å for both images. An ordered structure is observed but it is impossible to resolve the individual *n*-decanol molecule. In Figure A1(a), the width of the bright band measured at an angle 60 ° with respect to the dark trough corresponds to the length of two *n*-decanol molecules. This interpretation cannot be done without the results presented in Chapter 2. By examining these two images alone, it is difficult to deduce the orientation of the molecules on the graphite surface.

Figures A2(a) and (b) show a dual bias imaging of the adsorbed layer. The results are similar to the those observed when imaging at the pure liquid *n*-decanol/graphite interface. A strong voltage dependent imaging shows that at lower voltage, the graphite lattice can be imaged without disturbing the adsorbed molecules. Although we can not identify the structure in these images, they clearly show that in a narrow range bias voltages, the tunneling probability can change dramatically.

Reference to Appendix A

[A1] J. P. Rabe, private communications, Baltimore 1990.

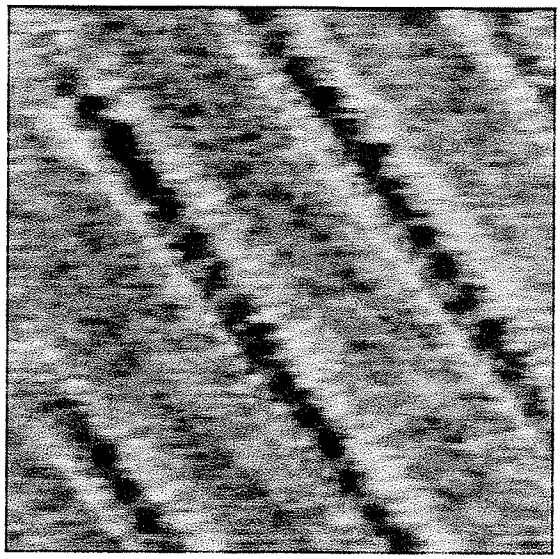

(a)

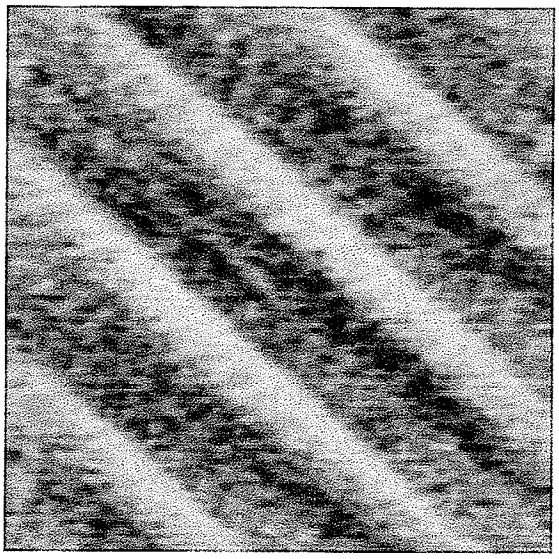

(b)

Figure A1 80 Å x 80 Å STM images of *n*-decanol taken at oil/graphite interface.

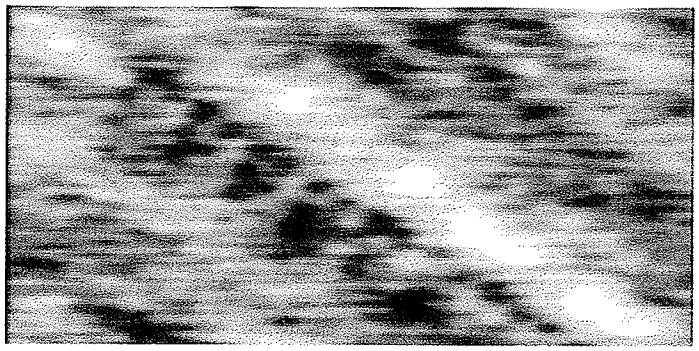

(a) 0.42 V

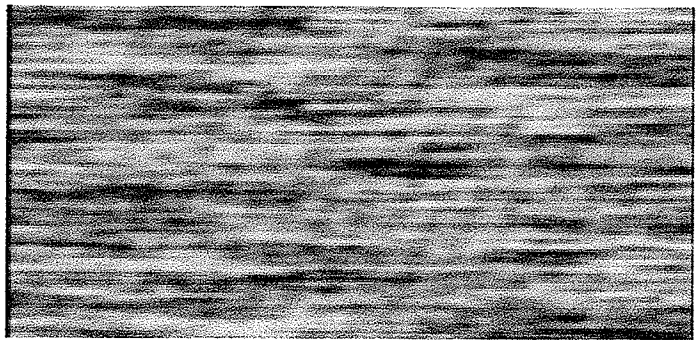

(b) 0.2 V

Figure A2 Dual bias imaging of *n*-decanol. Image size is 80 Å x 32 Å.

Appendix B

Imaging Cu-Phthalocyanine on Gold

Here we present the results of Cu-phthalocyanine (Cu-phth) on gold surface, a minute contribution to the *STM-AFM and Biological 'Objects' Workshop 1992*, organized and financed by the Fourmentin-Grilbert Scientific Foundation. The sample was provided by the Maurice E. Muller-Institüt.

The Cu-phth molecules have been observed to adsorbed on Ag [B1], Cu(100) [B2] and GaAs(100) [B3] in UHV with the STM. A drawing of the Cu-phth molecule is shown in Figure A1. The size of the molecule is approximately 20 Å. Imaging of Cu-phth on graphite in air was previously done by first acidified the graphite surface and let a base-substituted Cu-phth to bind on the substrate [B4]. Here we examined the adsorption of the Cu-phth molecules on Au in an aqueous solution.

The Cu-phth is first dissolved in *n*-octanol solution. A few drops of this solution is then put on top of an epitaxially grown Au film on mica. Figures A2(a) and (b) show the STM images obtained in the aqueous solution. The Au surface seems to be saturated with the Cu-phth molecules. The size of the bright 'circles' range from 20 Å to 30 Å. This could be due to the electronic perturbation of multilayers of Cu-phth molecules, so that they appear larger in size. We do not observe these large features when imaging the Au in pure *n*-octanol solution. Note that the images are taken with voltage above 1 V, below this voltage the image reveals the Au surface. Figures A3(a) and (b) show two 600 Å x 600 Å areas scanned at two different voltages. At 1.2 V, the Cu-phth molecules can be seen to adsorbed on the Au terraces. At 0.5 V however, the surface appears to be free from the adsorbates. This strong voltage dependence

characteristic was also observed with Cu-phth on surfaces in UHV [B1, B2]. More detail interpretations may be made upon comparison with results submitted by other research groups to the workshop.

Reference to Appendix B

[B1] J. K. Gimzewski, E. Stoll and R. R. Schlittler, *Surf. Sci.* 181 (1986) 267.

[B2] P. H. Lippel, R. J. Wilson, M. V. Miller, Ch. Wöll and S. Chiang, *Phys. Rev. Lett.* 62 (1989) 171.

[B3] R. Möller, R. Coenen, A. Esslinger and B. Koslowski, *J. Vac. Sci. Technol.* A8 (1990) 659.

[B4] M. Pomerantz, A. Aviram, R. A. McCorkle, L. Li and A. G. Schrott, *Science* 255 (1992) 1115.

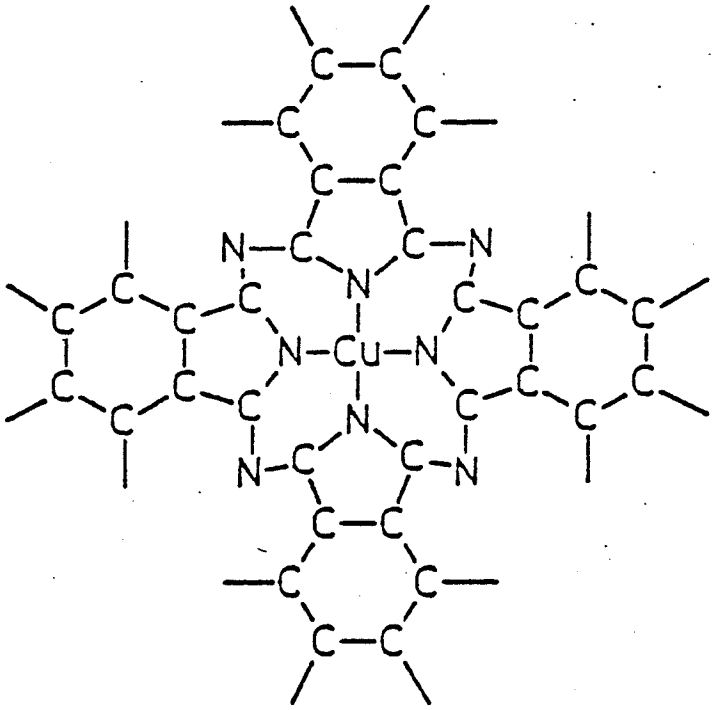

Figure B1 The Cu-Phthalocyanine Molecule.

(a) 160 Å x 160 Å

(b) 320 Å x 250 Å

Figure B2 STM images of Cu-Phth on gold at (a) 1.3 V and (b) 1.7 V.

(a) 600 Å x 600 Å

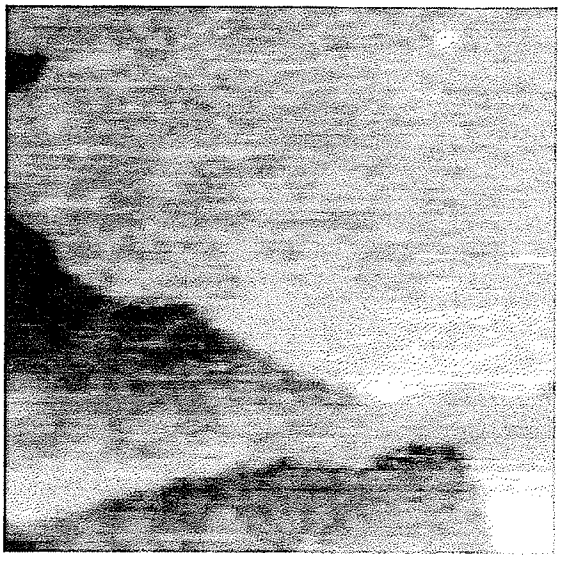

(b) 600 Å x 600 Å

Figure B3 Image at two voltages (a) 1.2 V and (b) 0.5 V, both 0.45 nA.

Appendix C

Publications & Conference Proceedings Resulting from Work to Date

[1] G. C. McGonigal, R. H. Bernhardt, Y. H. Yeo and D. J. Thomson, *AIP Conference Proceedings*, ed. H. K. Wickramasinghe 241 (1991) 190.

[2] G. C. McGonigal, R. H. Bernhardt, D. J. Thomson and Y. H. Yeo, *J. Vac. Sci. Technol.* B9 (1991) 1107.

[3] Y. H. Yeo, K. Yackoboski, G. C. McGonigal and D. J. Thomson, *J. Vac. Sci. Technol.* A10 (1992) 600.

[4] K. Yackoboski, Y. H. Yeo, G. C. McGonigal and D. J. Thomson, *Ultramicroscopy*, 42-43 (1992) 963.

[5] Y. H. Yeo, G. C. McGonigal, K. Yackoboski, C. X. Guo and D. J. Thomson, *J. Phys. Chem.* 96 (1992) 6110.

[6] Y. H. Yeo, G. C. McGonigal and D. J. Thomson, *Langmuir* 9 (1993) 649.

[7] Y. H. Yeo and D. J. Thomson, to be published in *J. Phys. Chem.*.